# REPORT DOCUMENTATION PAGE

Form Approved
OMB No. 0704-0188



| 1. REPORT DATE (DD-MM-YYYY) | 2. REPORT TYPE | 3. DATES COVERED (From - To) |
|---|---|---|
| June 2004 | Journal Article | 2004 |

4. TITLE AND SUBTITLE

Pseudoelastic SMA Spring Elements for Passive Vibration Isolation: Part II – Simulations and Experimental Correlations

5a. CONTRACT NUMBER

5b. GRANT NUMBER

5c. PROGRAM ELEMENT NUMBER

6. AUTHOR(S)

Dimitris C. Lagoudas, Mughees M. Khan, John J. Mayes,* and Benjamin K. Henderson**

5d. PROJECT NUMBER

5e. TASK NUMBER

5f. WORK UNIT NUMBER

7. PERFORMING ORGANIZATION NAME(S) AND ADDRESS(ES)

Department of Aerospace Engineering
Texas A&M University
College Station, TX 77843

*V-22 Structure and Development
Airframe Systems
Bell Helicopter, Textron
Fort Worth, TX 76101

8. PERFORMING ORGANIZATION REPORT NUMBER

9. SPONSORING / MONITORING AGENCY NAME(S) AND ADDRESS(ES)

**AFRL/VSSV
3550 Aberdeen Ave SE
Kirtland AFB, NM 87117-5776

10. SPONSOR/MONITOR'S ACRONYM(S)

11. SPONSOR/MONITOR'S REPORT NUMBER(S)

12. DISTRIBUTION / AVAILABILITY STATEMENT

Approved for public release; distribution is unlimited.



13. SUPPLEMENTARY NOTES

Journal of Intelligent Material Systems and Structures, Vol. 15—June 2004, pp. 443-470.

14. ABSTRACT

In Part II of this two-part study, system simulations and experimental correlations of a Shape Memory Alloy (SMA) based vibration isolation device (briefly described in Part I) has been presented. This device consists of layers of preconstrained SMA tubes undergoing pseudoelastic transformations under transverse dynamical loading. In Part II, detailed description of the prototype vibration isolation device, its experimental setup, and actual experimental test results are presented. An extensive parametric study has been conducted on a nonlinear hysteretic dynamical system, representing this vibration isolation device utilizing a physically based simplified SMA model and a Preisach model (an empirical model based on system identification) developed in Part I. Both the physically based simplified SMA model and the modified Preisach model have been utilized to perform experimental correlations with the results obtained from actual testing of the device. Based on the investigations, it has been shown that variable damping and tunable isolation response are major benefits of SMA pseudoelasticity. Correlation of numerical simulations and experimental results has shown that large amplitude displacements causing phase transformations of SMA components present in such a device are necessary for effective reduction in the transmissibility of such dynamical systems. It has also been shown that SMA-based devices can overcome performance trade-offs inherent in typical softening spring-damper vibration isolation systems. In terms of numerically predicting the experimental results, it has been shown that the Preisach model gave relatively accurate results due to better modeling of the actual SMA tube behavior. However for a generic parametric study, the physically based simplified SMA model has been found to be more useful as it is motivated from the constitutive response of SMAs and hence, could easily incorporate different changes in system conditions.

15. SUBJECT TERMS

Shape memory alloys (SMAs), pseudoelasticity, hysteresis, Preisach, system identification, passive vibration isolation, damping, dynamic system

| 16. SECURITY CLASSIFICATION OF: | | | 17. LIMITATION OF ABSTRACT | 18. NUMBER OF PAGES | 19a. NAME OF RESPONSIBLE PERSON |
|---|---|---|---|---|---|
| a. REPORT | b. ABSTRACT | c. THIS PAGE | | | Benjamin K. Henderson |
| Unclassified | Unclassified | Unclassified | Unlimited | 29 | 19b. TELEPHONE NUMBER (include area code) 505-853-6712 |

# Pseudoelastic SMA Spring Elements for Passive Vibration Isolation: Part II – Simulations and Experimental Correlations

DIMITRIS C. LAGOUDAS,[1,*] MUGHEES M. KHAN,[1] JOHN J. MAYES[2] AND BENJAMIN K. HENDERSON[3]

[1]*Department of Aerospace Engineering, Texas A&M University, College Station, TX 77843, USA*
[2]*V-22 Structure and Development, Airframe Systems, Bell Helicopter, Textron, Fort Worth, TX 76101, USA*
[3]*Air Force Research Laboratory/VSSV, Kirtland AFB, NM 87117, USA*

**ABSTRACT:** In Part II of this two-part study, system simulations and experimental correlations of a Shape Memory Alloy (SMA) based vibration isolation device (briefly described in Part I) has been presented. This device consists of layers of preconstrained SMA tubes undergoing pseudoelastic transformations under transverse dynamical loading. In Part II, detailed description of the prototype vibration isolation device, its experimental setup, and actual experimental test results are presented. An extensive parametric study has been conducted on a nonlinear hysteretic dynamical system, representing this vibration isolation device utilizing a physically based simplified SMA model and a Preisach model (an empirical model based on system identification) developed in Part I. Both the physically based simplified SMA model and the modified Preisach model have been utilized to perform experimental correlations with the results obtained from actual testing of the device. Based on the investigations, it has been shown that variable damping and tunable isolation response are major benefits of SMA pseudoelasticity. Correlation of numerical simulations and experimental results has shown that large amplitude displacements causing phase transformations of SMA components present in such a device are necessary for effective reduction in the transmissibility of such dynamical systems. It has also been shown that SMA-based devices can overcome performance trade-offs inherent in typical softening spring-damper vibration isolation systems. In terms of numerically predicting the experimental results, it has been shown that the Preisach model gave relatively accurate results due to better modeling of the actual SMA tube behavior. However, for a generic parametric study, the physically based simplified SMA model has been found to be more useful as it is motivated from the constitutive response of SMAs and hence, could easily incorporate different changes in system conditions.

*Key Words:* shape memory alloys (SMAs), pseudoelasticity, hysteresis, Preisach, system identification, passive vibration isolation, damping, dynamic system

## INTRODUCTION

SHAPE Memory Alloys (SMAs) appear to be viable candidates for use in the field of vibration isolation as mentioned in Part I of this two-part paper due to the nature of the pseudoelastic behavior (Wayman, 1983; Otsuka and Shimizu, 1986) exhibited when a SMA material is loaded at temperatures greater than the austenitic finish temperature.

In work done by Yiu and Regelbrugge (1995), the behavior of SMA springs designed to act as an on-orbit soft mount isolation system for a momentum wheel assembly has been numerically investigated with the added benefit of precision alignment through the utilization of the SMA shape-memory effect. In work done by Feng and Li (1996) some effects of pseudoelasticity on vibration isolation with qualitative experimental validation of theory have been explored. They have observed a left shift in the response peak towards lower frequencies due to the softening behavior in the SMA response due to phase transformation from $A \rightarrow M$. In work done by Collet et al. (2001) similar conclusions have been drawn for a SMA beam acting as a vibration isolation device along with qualitative experimental observation by performing dynamical testing of the SMA beam.

However, the above mentioned publications have not considered a wide range of conditions like SMA undergoing complete phase transformation, reverse phase transformation from $M \rightarrow A$ and the affect that different system parameters like mass, initial conditions, and amplitude of excitation have on the dynamic response of a SMA-based vibration isolation system. A noted exception is a recent theoretical study by Bernardini and Vestroni (2002), where non-

*Author to whom correspondence should be addressed.
E-mail: dlagoudas@aero.tamu.edu



1045-389X/04/06 0443–28 $10.00/0 DOI: 10.1177/1045389X04041530

linear, dynamic nonisothermal response of pseudoelastic shape-memory oscillators have been presented. Softening as well as hardening behavior is noted as the SMA undergoes partial and full phase transformation under varying force excitation amplitude, hysteresis shape, and temperature. Based on the work done by Bernardini and Vestroni (2002), Lacarbonara et al. (2001) have studied periodic and nonperiodic thermomechanical response of a shape-memory oscillator and considered both isothermal and nonisothermal conditions under forced vibration and presented a rich class of solutions and bifurcations including jump phenomena, pitch fork, period doubling, complete or incomplete bubble structures with a variety of nonperiodic responses. Results presented in Lacarbona et al. (2001) show that for the range of parameters investigated, the nonisothermal and isothermal responses were similar to each other.

Based on the work done on SMA-based dynamical systems mentioned in the above publications, there is a need to explore the effects of SMA pseudoelasticity on vibration isolation by performing actual experimental correlations and conducting parametric studies under various dynamic loading conditions on an actual SMA-based vibration isolation device.

In Part II of this two-part paper series the effects of complete and partial pseudoelastic phase transformations on a SMA-based vibration isolation device are investigated with respect to system parameters like mass, amplitude of input excitation and initial conditions utilizing the models developed in Part I along with experimental correlations of actual dynamical testing of a pseudoelastic SMA vibration isolation device. Outline of this paper is as follows: first, description of the vibration isolation device which consists of SMA tubes undergoing pseudoelastic transformations under transverse loading is presented. Actual experimental test results are also presented followed by description of a SMA-based system model of the prototype device where the SMA behavior is predicted by the two models developed in Part I. Abovementioned issues are addressed by presenting numerical simulations of a generic pseudoelastic SMA spring-mass system followed by simulations of a nonlinear hysteretic dynamical system based on the prototype device. Finally, experimental correlations of model predictions with the experimental results are presented followed by concluding remarks for the two-part paper series.

## DESCRIPTION OF SMA VIBRATION ISOLATION EXPERIMENT

For this work, an experimental device was built to determine the effectiveness of SMAs when the pseudoelastic response is used in a dynamic system for passive vibration isolation. SMA tubes were chosen to investigate the validity of SMA spring elements as vibration isolators due to availability and ease in manufacturing of SMA tubes. In this device, layers of preconstrained thin-walled SMA tubes loaded in a transverse direction in compression were used to support the mass, which was subjected to base excitations. The tubes were acquired from SMA, Inc. and were manufactured from Nitinol with a diameter of approximately 6 mm and a wall thickness of approximately 0.17 mm. The tubes used in the experiment were cut to 10 mm in length.

The experimental testing was conducted at the Air Force Research Laboratory, Kirtland AFB, NM. The shaker configuration with the SMA spring-mass system attached is shown in Figure 1, where SMA tubes have been shown as nonlinear springs. Figure 2 shows the actual setup along with the prototype device.

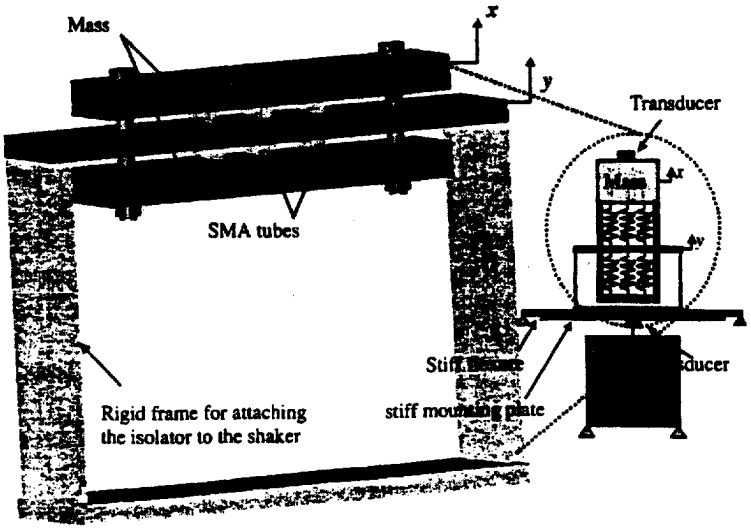


*Figure 1. Schematic of shaker and SMA spring-mass isolation system as tested.*

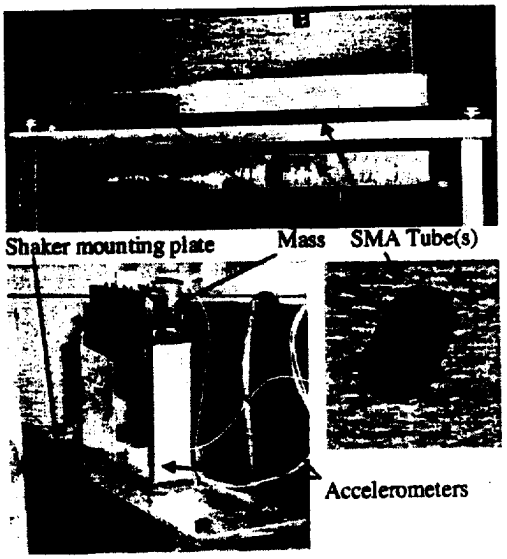


***Figure 2.*** *SMA device vibration test setup.*

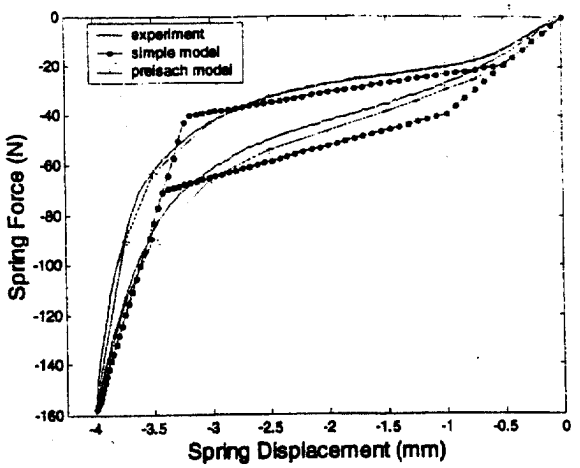


***Figure 3.*** *Comparison of calibrated models with experimental response of a SMA tube used in the vibration isolation device.*

***Table 1. Test matrix for SMA spring-mass system.***

| Case No. | Mass (kg) | SMA Tubes 4 | SMA Tubes 6 | Tube Pre-comp. pc I 20% | Tube Pre-comp. pc II 26% | Loading (gs) 1/4 | 1/2 | 3/4 | 1 |
|---|---|---|---|---|---|---|---|---|---|
| 1 | 0.5 | x | | x | | x | x | x | x |
| 2 | 0.8 | x | | x | | x | x | x | x |
| 3 | 1.0 | x | | x | | x | x | x | x |
| 4 | 1.2 | x | | x | | x | x | x | x |
| 5 | 1.5 | x | | x | | x | x | x | x |
| 6 | 0.5 | | x | x | | x | x | x | x |
| 7 | 0.8 | | x | x | | x | x | x | x |
| 8 | 1.0 | | x | | x | x | x | x | x |
| 9 | 0.5 | x | | | x | x | x | | |
| 10 | 0.5 | | x | x | | x | x | | |

The excitation during the testing was provided by a VTS-100 electromagnetic shaker and accompanying power amplifier controlled by a Hewlett-Packard 35665A Dynamic Signal Analyzer. Dynamic excitation was measured using two PCB 336C04 accelerometers, with one located on the shaker table and the other located on the SMA spring-mass system. Constant acceleration amplitude frequency sweeps were used as the input waveform and were controlled via a feedback loop using the accelerometer on the shaker table as the input source. Output acceleration was also measured by a signal analyzer and the ratio of the magnitude of the output to the input accelerations was processed to create a frequency domain transfer function for the system. Details of the experimental setup and various experimental cases have been presented in detail in work done by Mayes and Lagoudas (2001) and Mayes (2001).

The experiment was designed so that the SMA tubes operated in pairs to provide resistance to both tension and compression for the system as a whole while always being under some compression on an individual basis. The initial compression of the tubes is referred to as the precompression and given as a percentage of the initial undeformed diameter of the tubes. This precompression will dictate the point about which the tubes will operate in the transition region of their pseudoelastic response, and variations in the amount of precompression will affect both the stiffness of the system and the energy absorbed due to SMA hysteresis. A typical force–displacement relation for the SMA tube modeled as a SMA compression spring is shown in Figure 3 along with the calibrated model responses. This data represents the structural response of a SMA tube, not the constitutive response of a SMA itself and has been discussed in detail in Part I and reproduced in Part II for the sake of continuity.

During the experiments, several of the parameters were varied to determine their effect on the behavior of the system. The number of SMA tubes (compression springs), the mass to be isolated and the loading input into the system were all varied following the test matrix presented in Table 1 to obtain a broad spectrum of performance for the SMA-based vibration isolation device. An important parameter of interest was determining the effect of changes in the precompression of the SMA tubes on the dynamic response of the system. Since the amplitude of motion for this series of tests was relatively small compared to the amplitude equivalent to the undeformed diameter of the SMA tubes, the degree of transformation was mostly influenced by the amount of precompression placed on the tubes. After setting the precompression, the SMA tubes would operate in minor loop hysteresis cycles about the preset precompression point without much deviation in displacement. Naturally, had the loading amplitude been greater, this would not necessarily be true, however, for this system it was possible to manipulate the degree of transformation of the SMA tubes by adjusting the precompression

As noted in Table 1, two different amounts of precompression were tested, 20% and 26% reduction in length compared to the original undeformed diameter. These two levels of precompression are here-after referred to as "*pc I*" and "*pc II*" precompression, respectively. Testing of Cases 1–7 were all performed at "*pc I*" precompression levels. Cases 8 and 9 were performed at "*pc II*" precompression levels and the results of this series of tests were then compared to the corresponding results from Cases 4 and 7.

## Experimental Results

Results from this series of experiments are shown in Figures 4–9. Figures 4–6 show the results for two pairs of SMA tubes, or four total, and Figures 7–9 show the results for three pairs of SMA tubes, or six total.

### *EFFECT OF CHANGES IN LOADING ON SYSTEM RESPONSE*

For Figures 4–6, where four SMA tubes were used, the mass is increased for each successive figure and the increase in mass results in a lower resonance frequency, similar in magnitude to the decrease in resonant frequency expected from a linear analysis. However, for a constant mass, there is an additional decrease in resonant frequency as the loading on the system increases. This reduction in frequency can be as much as 25% (Figure 6) but is usually in the range of 5–10% (Figures 4 and 5). Accompanying the reduction

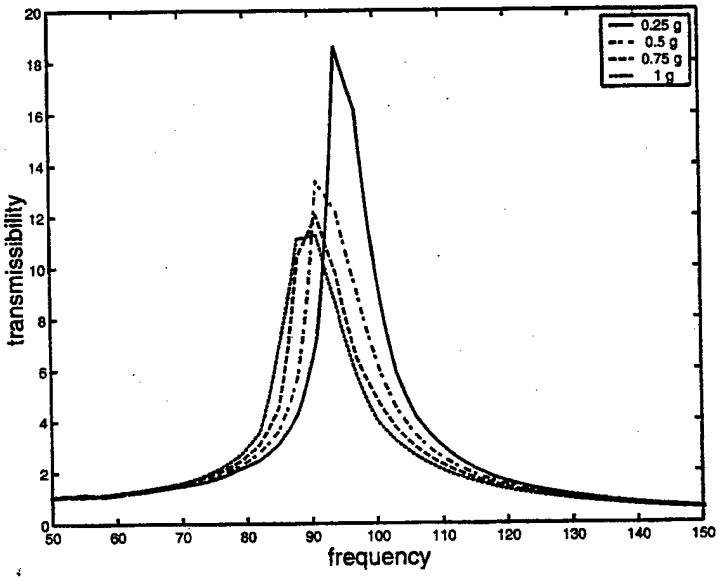


**Figure 4.** *Transmissibility for Case 1.*

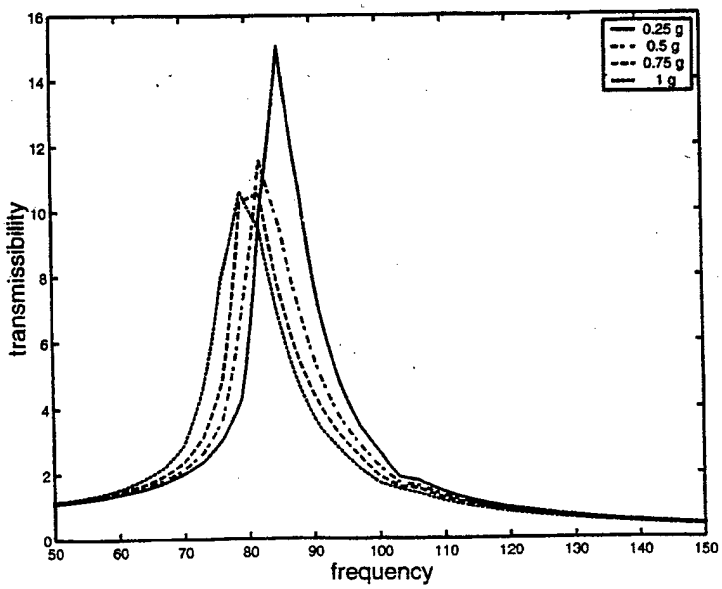


**Figure 5.** *Transmissibility for Case 2.*

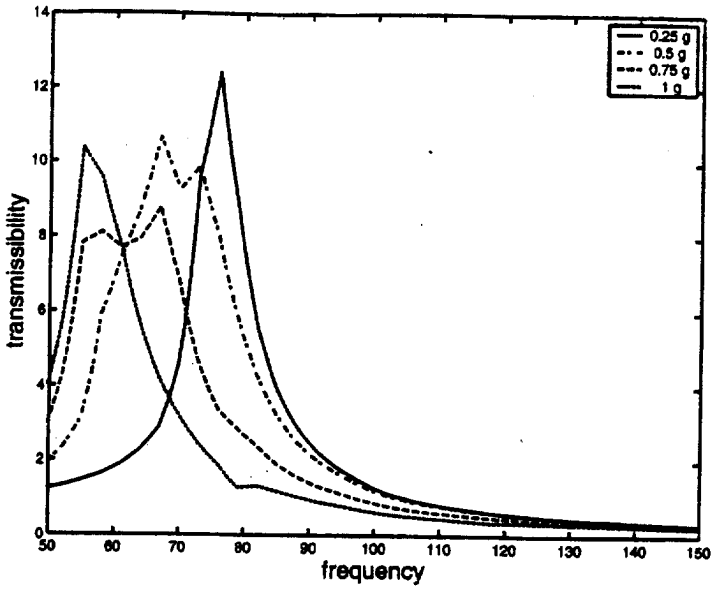


**Figure 6.** *Transmissibility for Case 3.*

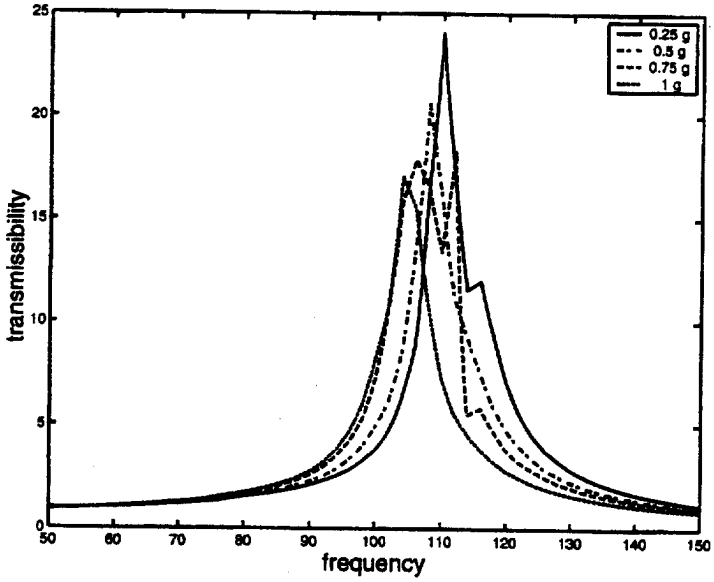


**Figure 7.** *Transmissibility for Case 6.*

in resonant frequency, there is also a consistent reduction in the magnitude of the resonant peak on the order of 30% (Figures 4–6). These reductions are a result of the nonlinear, hysteretic behavior of the SMA tubes and would not be seen in a similar linear system.

The same trends as discussed above are seen in Figures 7–9 for the experimental system with six SMA tubes. Again there is the expected decrease in resonant frequency for increasing mass. Similar to the results from the system using four tubes, there is also a reduction in resonant frequency as the loading applied to the system increases. From Figures 7–9 it can be seen that this reduction in resonant frequency is also of the order of 5–10%. Accompanying this reduction in resonant frequency is a reduction in the resonant amplitude as seen before. For Figure 9, this reduction is approximately 10%, however, for Figures 7 and 8 the reduction in resonant amplitude is much greater, of the order of 30–35%.

## *EFFECT OF CHANGES IN TUBE PRECOMPRESSION ON SYSTEM RESPONSE*

Referring to Figure 3, it is evident that changes in tube displacement will result in changes in the stiffness of the tube. However, given the nonlinear, hysteretic behavior of the pseudoelastic response of SMAs it was unclear what effect this would have on the response of the system. Therefore, experiments were conducted in which the precompression of the SMA tubes was

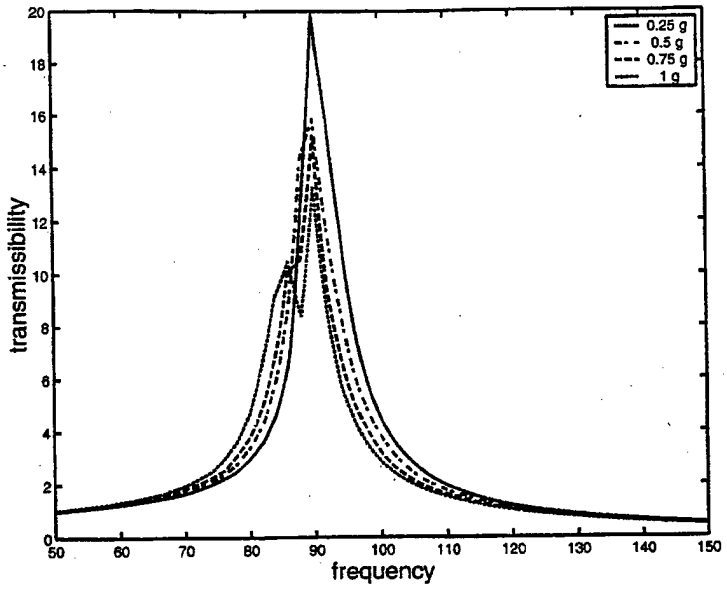


*Figure 8. Transmissibility for Case 7.*

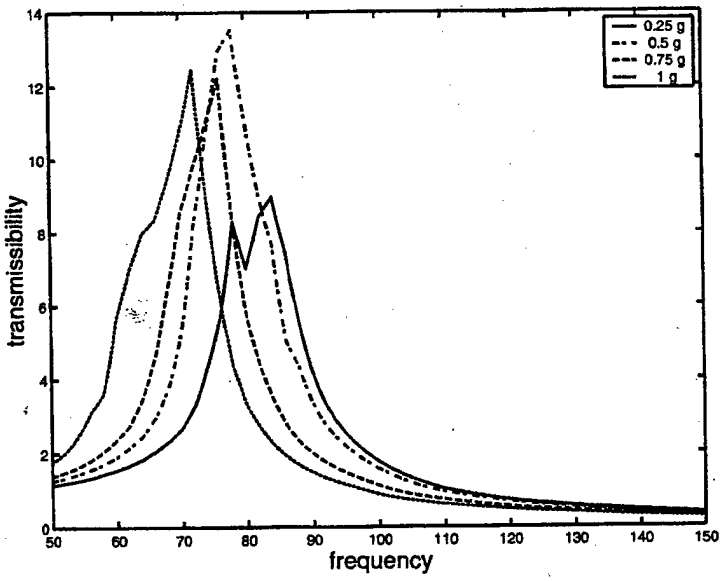


*Figure 9. Transmissibility for Case 8.*

changed while all other system parameters were held constant. The results of these tests are presented in Figures 10–13. Figures 10 and 11 show the effect of higher precompression for a four-tube system under 1/4 g and 1/2 g loading conditions, respectively. As shown, increasing the precompression results in an increase of resonant frequency by approximately 10–12%. Figures 12 and 13 show the similar results for a six-tube system under the same loading conditions. However, for this case the increase in resonant frequency is approximately 35–40% for the same increase in precompression. As shown, the effect of increasing the precompression was to increase the system stiffness for all cases, with a substantially larger effect seen in the six-tube system as compared to the four tube-system due to the additional stiffness provided by the increased number of tubes. Further experiments need to be performed, however it is expected that increases in the precompression up to approximately 50% will result in similar responses with increases above 50% resulting in a much stiffer system.

## SMA VIBRATION ISOLATION SYSTEM DESCRIPTION

Motivated by the need to model the SMA-based isolation device (Mayes and Lagoudas, 2001) presented in the last section, the simplified SMA model and the Preisach model (Part I) are utilized to solve a single

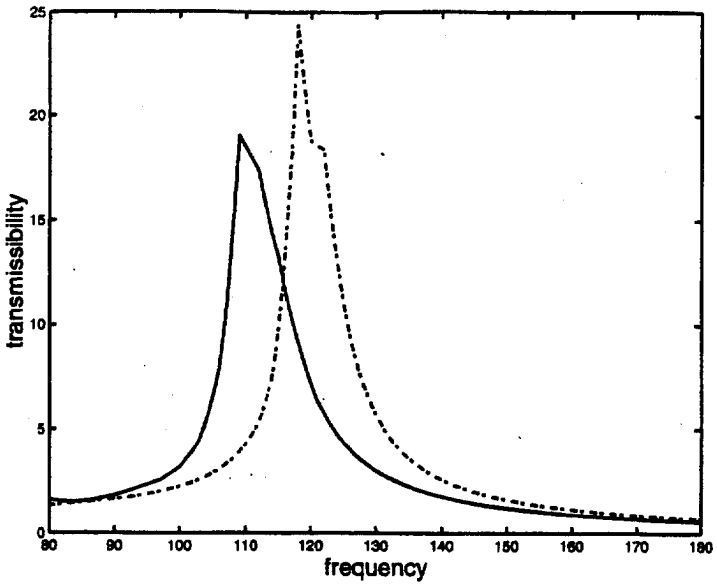


***Figure 10.*** *Transmissibility for Cases 7 (solid line) and 8 (dashed line).*

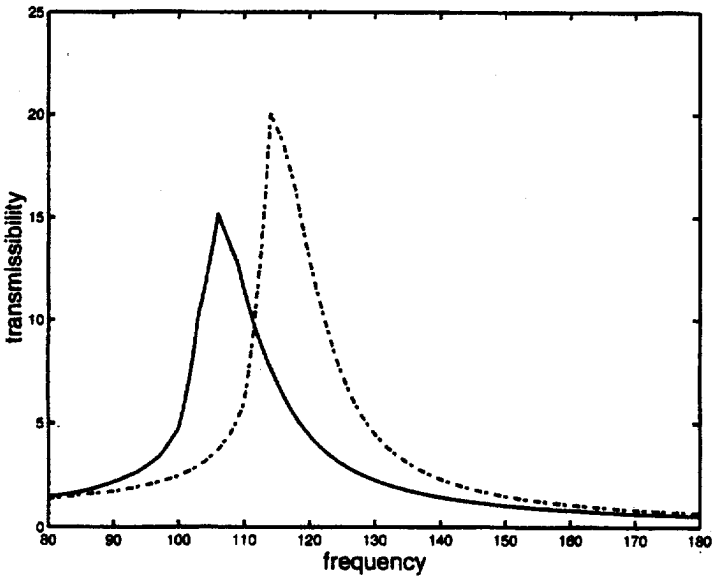


***Figure 11.*** *Transmissibility for Cases 7 (solid line) and 8 (dashed line).*

degree of freedom (SDOF) SMA spring-mass system (Lagoudas et al., 2002). To determine the effect of pseudoelastic SMA tubes on the response of the SMA-based vibration isolation system, the SMA tubes are modeled as nonlinear, hysteretic springs and are addressed as SMA springs in this two-part paper. Based on the prototype device shown in Figure 2, a schematic of the pseudoelastic SMA spring-mass system along with a free-body diagram of the mass being isolated is shown in Figure 14.

The system is excited by the motion of the supporting structure, denoted by ($y$) (base displacement). ($m$) is the mass to be isolated and ($x$) represents mass displacement. ($\delta_u$) and ($\delta_l$) represent displacement of the springs above and below the mass ($m$). The subscripts ($u$) and ($l$) represent "upper" and "lower" springs. Figure 14(b) shows the free body diagram of the SMA spring-mass system, where ($f_u^{SMA}$) and ($f_l^{SMA}$) represent force exerted by the upper and lower springs respectively. Note that for a configuration shown in Figure 14 with linear springs instead of SMA springs, all the springs would be modeled as springs in parallel and the spring force acting on mass ($m$) would be modeled as a single force. However, since SMA force response is displacement history dependent i.e., force exerted by a SMA is a "*functional*" of its displacement history, and is expressed as ($f^{SMA} = f^{SMA}[\delta]$). Therefore, for the given configuration, forces exerted by the SMA springs above the mass would be different from the forces exerted by the SMA springs below the mass as the springs

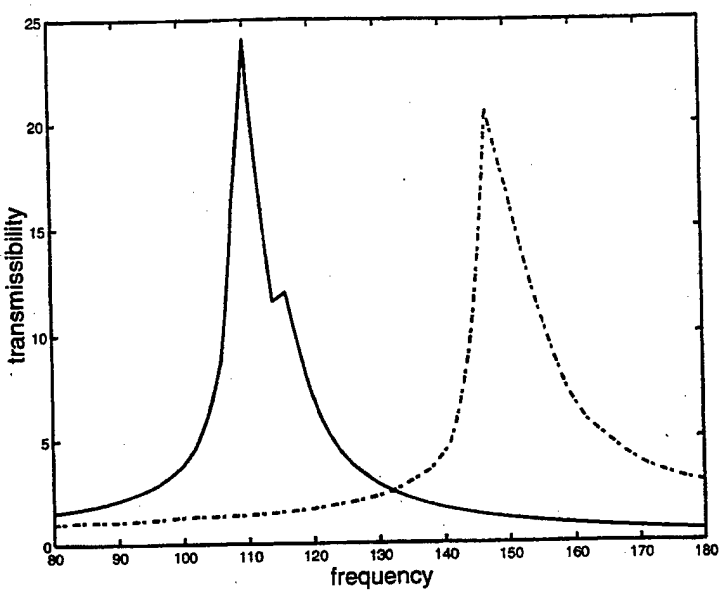


**Figure 12.** *Transmissibility for Cases 4 (solid line) and 9 (dashed line).*

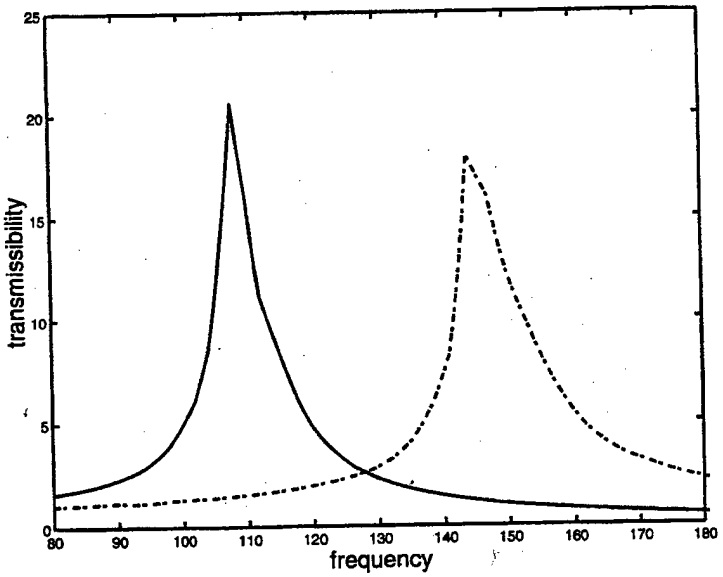


**Figure 13.** *Transmissibility for Cases 4 (solid line) and 9 (dashed line).*

above and below the mass would have different displacement histories due to the nonlinear hysteretic response of SMAs along with the different degree of pre-compressions as the device is assembled. From the free body diagram in Figure 14(b), the equation of motion or the conservation of linear momentum for the mass ($m$) can be determined as shown in Equation 1. ($\ddot{x}$) is the acceleration of the isolated mass and ($N_u$) and ($N_l$) refer to the number of springs on the upper or lower sides of the mass, respectively.

The forces exerted by the SMA springs not only account for the change in stiffness but also the damping introduced in the system due to pseudoelastic phase transformations. Force exerted by the upper springs

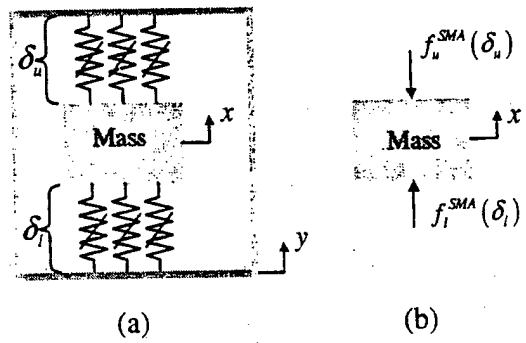


**Figure 14.** *(a) Schematic of pseudoelastic SMA spring-mass isolation system; (b) free body diagram of pseudoelastic SMA spring-mass isolation system.*

($f_u^{SMA}$) and lower springs ($f_l^{SMA}$) are determined by using the models developed in Part I and as mentioned above, these forces are dependent on the displacement of the springs, ($\delta_u$) and ($\delta_l$), and the displacement history of the springs as discussed previously. These displacements are related to ($x$) and ($y$) as shown in Equation (2).

$$m\ddot{x} = N_u f_u^{SMA}[\delta_u] - N_l f_l^{SMA}[\delta_l] \tag{1}$$

$$\delta_l = -\delta_u = x - y \tag{2}$$

Note that no viscous damping term also known as internal damping term has been included in Equation (1) as only damping due to hysteresis caused by SMA phase transformations is being investigated as the SMA tubes are always under a certain degree of precompression, i.e. the SMA tubes are operating in the middle of their phase transformation region as mentioned in the previous section. Based on the experimental setup and as mentioned above, same displacement and displacement histories have been considered for all the springs above the mass in Equation (1). The same has been considered for all the springs below the mass as shown in Equation (1) and any discrepancies in displacement and displacement histories of individual springs due to failure in maintaining appropriate tolerances during manufacturing have not been modeled.

Another important consideration is the effect of latent heat during the SMA exothermic ($A \rightarrow M$) and endothermic ($M \rightarrow A$) phase transformations. The heat released and absorbed to and from the environment during these phase transformations causes a change in the SMA temperature which leads to a change in the SMA constitutive response. Under isothermal conditions SMA pseudoelastic response is not affected by the change in SMA temperature due to latent heat, as the increase or decrease in temperature stabilizes with respect to the ambient temperature. However, for nonisothermal conditions SMA response is affected by the change in SMA temperature caused due to heat released and absorbed during phase transformations due to insufficient heat transfer between the SMA and the ambient environment. This results in a change in the SMA temperature. The SMA models were calibrated at the SMA tube response at room temperature (Figure 3). And as mentioned in Part I of this study, small changes in the shape of the SMA tube hysteresis were observed while testing the tube at temperatures ranging from 25 to 65°C with different cross-head displacement loading rates ranging from 0.016 to 0.3 mm/s. The tube response showed maximum 5% of increased hardening at higher testing temperatures and all loading rates as higher stresses are required to induce phase transformations (Figure 1, Part I). The small change in the force–displacement curves for different temperatures was attributed to the fact that only small parts of the SMA tube were undergoing phase transformation as discussed in Part I.

Based on the experiments and the FEA results (Part I), the authors have concluded that even though locally the increase or decrease in the SMA tube temperature due to latent heat of phase transformation may be significant especially under dynamic loading conditions, the overall structural response is not drastically affected. This is justified because heat conduction and heat convection to and from the tube will cause the tube to reach a steady state temperature close to the ambient environment at steady state dynamic response. And, as it will be shown later in this paper, for a given input excitation loading, as frequency increases the amount of SMA tube undergoing phase transformation decreases. Hence, temperature effects were assumed to be negligible for the SMA tubes used in this work and the tube response was modeled without considering release and absorption of latent heat during the SMA pseudoelastic deformations.

Excitation of the system is introduced through sinusoidal motion of the base of the device whose magnitude is determined by the desired loading to be placed on the structure for a given frequency sweep as mentioned in the previous section. Loading magnitude, ($a$) (Input loading level) is specified as a fraction of the acceleration due to gravity, ($g$). Loading frequency is specified in cycles per second, denoted as ($f$) (Excitation frequency). The acceleration due to gravity is taken as 9.81 m/s$^2$. The magnitude of displacement ($Y$), necessary to achieve a required acceleration at a given frequency is determined by the relationship shown in Equation (3), given that the motion is sinusoidal and periodic. Equation 4 gives an expression for a sinusoidal displacement input.

$$Y = \frac{ag}{(2\pi f)^2} \tag{3}$$

$$y = Y\sin(2\pi f t) \tag{4}$$

The transmissibility, $TR$, (Transmissibility) of the system, is a measure of the force or motion transmitted through the system. Displacement transmissibility has been considered for the analysis that is shown mathematically in Equation (5).

$$TR = \frac{|x|}{|y|} \tag{5}$$

$$\tag{6}$$

With the response of the SMA springs defined, it is now possible to model the system as depicted in Figure 14 and described by Equation (1). The simulation

of the dynamic system was at first implemented in a MATLAB (The Mathworks Incorporated, 1999) environment and later on converted to a C/C++ environment to develop an efficient simulation tool. Time history response of the system was calculated using a Newmark integration scheme (Newmark, 1959) with time step and weighting factors determined to ensure stability of both the integration scheme, the simplified SMA model and the modified Preisach model describing the SMA spring element behavior. The reader is referred to Lagoudas et al. (2001) for details on verification of the Newmark Scheme. For the sake of completeness only a brief description is presented below.

The time integration is done by the constant-average acceleration method, a variant of the Newmark scheme. For $t = t_n$ the Newmark scheme is defined by:

$$x_{n+1} = x_n + \Delta t \dot{x}_n + \frac{1}{2}(\Delta t)^2((1-\gamma)\ddot{x}_n + \gamma \ddot{x}_{n+1}) \quad (7)$$

$$\dot{x}_{n+1} = \dot{x}_n + \Delta t((1-\alpha)\ddot{x}_n + \alpha \ddot{x}_{n+1}) \quad (8)$$

The constant-average acceleration method (trapezoidal rule) is obtained for $\alpha = 1/2$, $\gamma = 1/2$. The selection of this second-order implicit method was governed by the highly nonlinear nature of the differential equation describing the system. For a linear system, this scheme conserves the total energy of the system, allowing the high-frequency response to be simulated without any numerical damping, and is unconditionally stable. The same scheme is used to solve the nonlinear, hysteretic SMA spring-mass system based on the understanding that unconditional stability holds for certain nonlinear systems. However, no proof of stability of the integration scheme for this type of nonlinear systems is available. For a detailed discussion on time-integration schemes, the reader is referred to Hughes (1987).

## PARAMETRIC STUDY AND SYSTEM SIMULATION

### Single Pseudoelastic SMA Spring-mass System using the Physically Based Simplified SMA Model

To qualitatively identify the effects of material softening, precompression and hysteresis on SMA-based vibration isolation, a single pseudoelastic SMA spring-mass system has been investigated as a first step toward performing simulations of the system given by the schematic in Figure 14. Only the simplified SMA model has been used for this qualitative parametric study. Schematic of a basic SMA spring-mass system is given in Figure 15. For a fixed excitation of $a = 0.25$, with only one single spring ($N_u = 1$ and $N_i = 0$ in Equation (1)), Figure 16 shows effects of varying mass on the transmissibility of a simple SMA spring-mass system. Not only does the natural frequency of the system decrease as the mass increases, but the transmissibility of the system also reduces. Reduction in transmissibility is

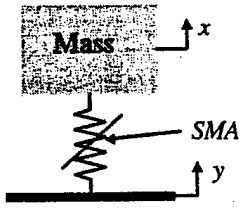


*Figure 15. Schematic of a simple pseudoelastic SMA spring-mass system.*

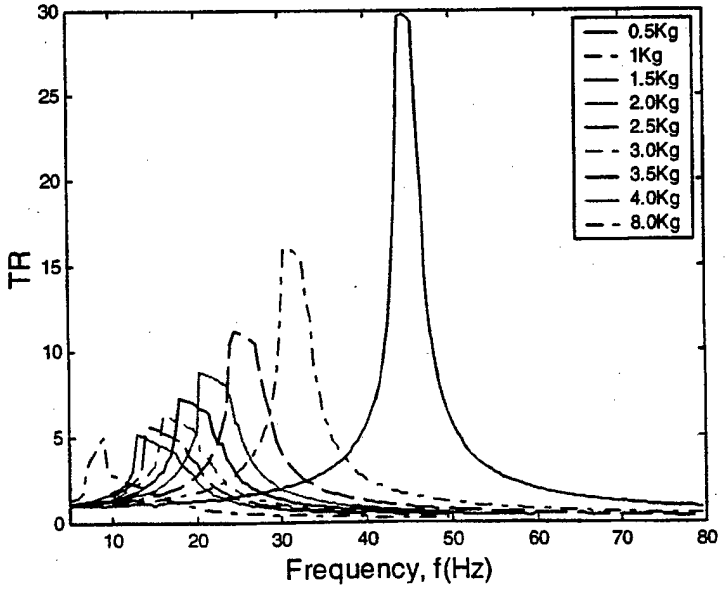


*Figure 16. Effects of varying mass on transmissibility.*

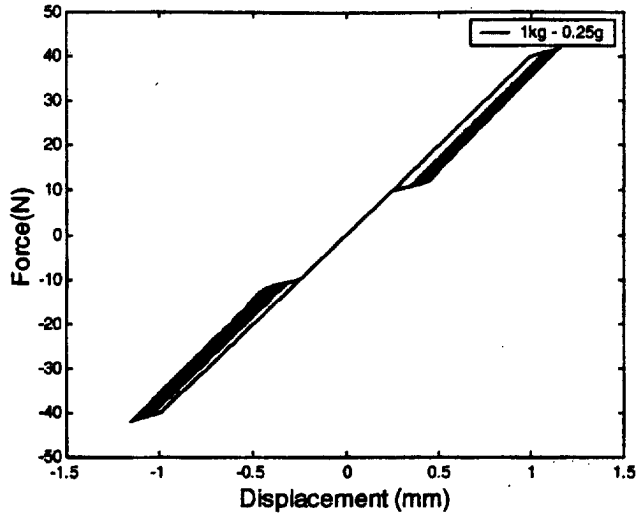


***Figure 17.*** *Force–displacement response for 1 kg mass with 0.25 g excitation.*

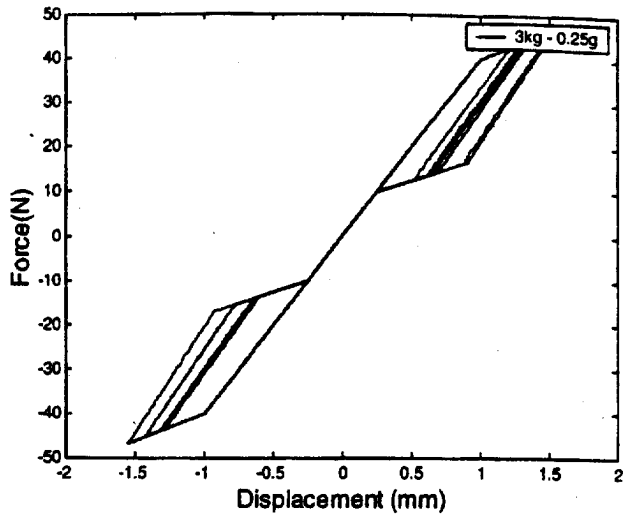


***Figure 19.*** *Force–displacement response for 3 kg mass with 0.25 g excitation.*

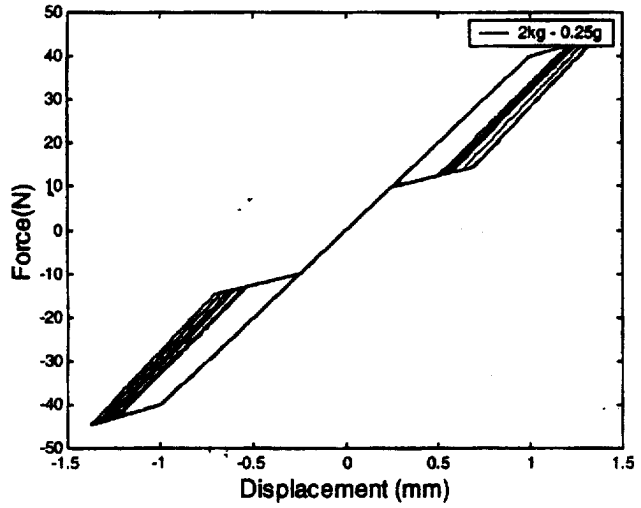


***Figure 18.*** *Force–displacement response for 2 kg mass with 0.25 g excitation.*

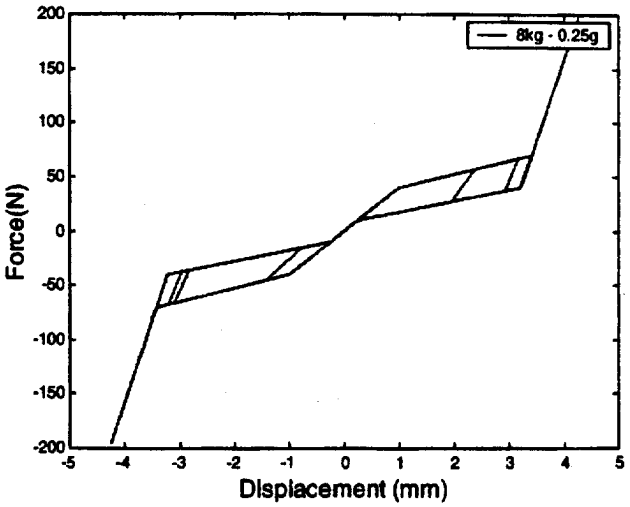


***Figure 20.*** *Force–displacement response for 8 kg mass with 0.25 g excitation.*

attributed to the relative increase in spring displacement with increasing mass, causing phase transformation along with the hysteresis. Figures 17–20 shows force–displacement diagrams of the spring for mass values of 1, 2, 3 and 8 kg at their respective resonance conditions. Increase in mass after inducing full phase transformation does not yield a significant decrease in transmissibility (see Figures 16 and 20) as the spring starts behaving like a trilinear spring, along with the hysteresis effect, an important thing to note is that increasing the mass any higher after undergoing full phase transformation minimizes the effect of the hysteresis and the reduction in transmissibility is relatively small.

Effects of varying excitation on transmissibility for mass of 1, 2 and 3 kg are given in Figures 21–23. For all the three masses, at lower excitations the natural frequency does not shift as the spring loads and unloads with a stiffness very close to the stiffness of the austenitic phase due to small phase transformation, however a reduction in transmissibility is observed because of the hysteresis.

An increase in excitation increases the relative displacement of the spring causing greater phase transformation. Higher phase transformation magnifies the softening behavior of the SMA, this results in lower natural frequency of the system. However, further increase in excitation results in complete phase transformation into the martensitic region. Since the stiffness of this spring is much higher in the martensitic phase the natural frequency of the system starts to increase. An important observation has been the discontinuous nature of the transmissibility curves for the single spring system, which occurs when the spring starts phase transformation from the martensitic phase into the austenitic phase or vice versa causing a sudden

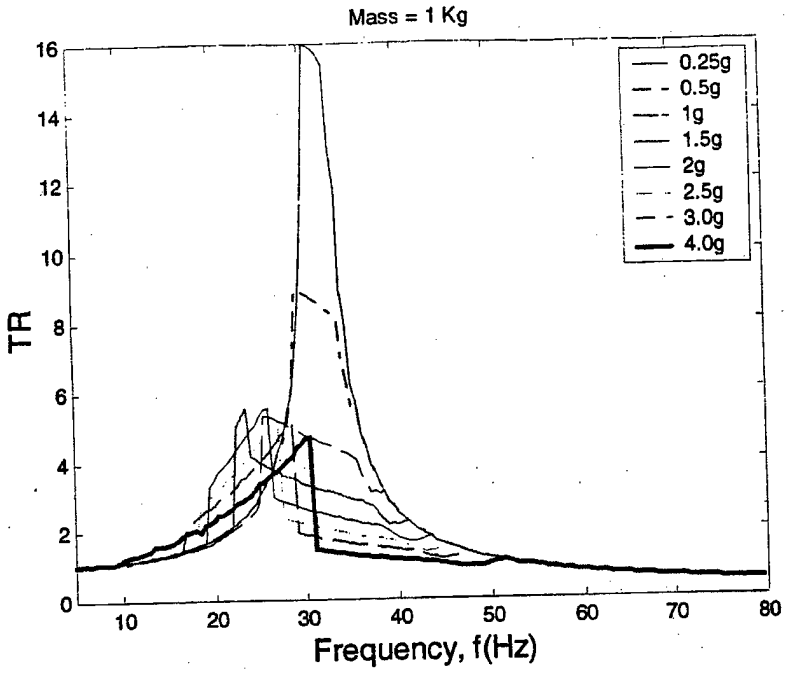


**Figure 21.** *Effects of varying excitation on transmissibility for 1 kg mass.*

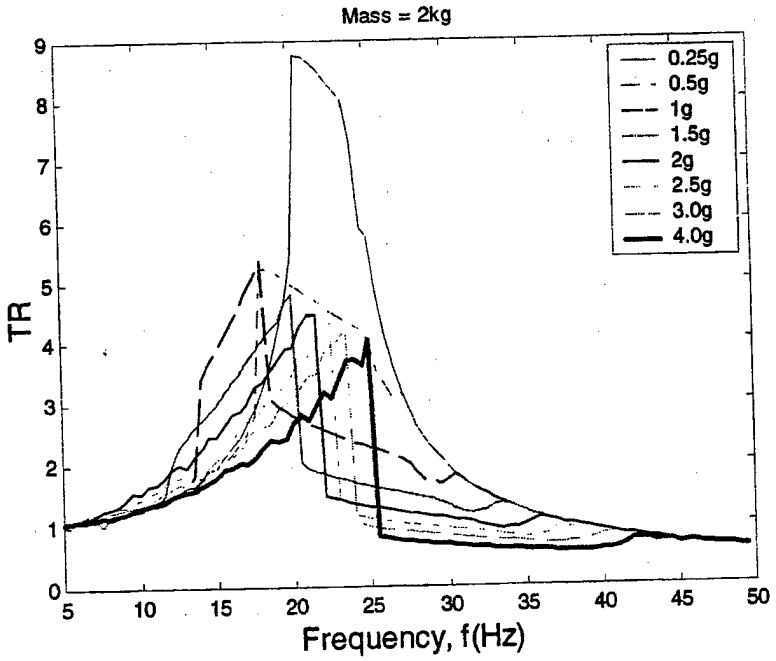


**Figure 22.** *Effects of varying excitation on transmissibility for 2 kg mass.*

change in stiffness. The sudden change in stiffness upon loading or unloading which is observed at the onset of the hysteretic response as shown in Figures 24 and 25 (unloading case) gives a lower transmissibility. The discontinuous nature of the transmissibility curves for a spring exhibiting hardening or softening nonlinearity similar to the pseudoelastic SMA response undergoing $M \rightarrow A$ and $A \rightarrow M$ phase transformations is referred in the literature as the *jump phenomenon* (Meriovitch, 1975; Nayfeh and Mook, 1979). These significant jumps are attributed to the multivaluedness of the response curves, which are due to the spring nonlinearity and have been observed experimentally (Collet et al., 2001). The reader is referred to expositions on the jump phenomenon for nonlinear springs in Nayfeh and Mook (1979) for further explanations. For the model presented in this work (Part I) representing pseudoelastic SMA phase transformations with sudden change in stiffness, namely the simplified model and its correlation with the mechanism-based hysteretic nonlinear response, the

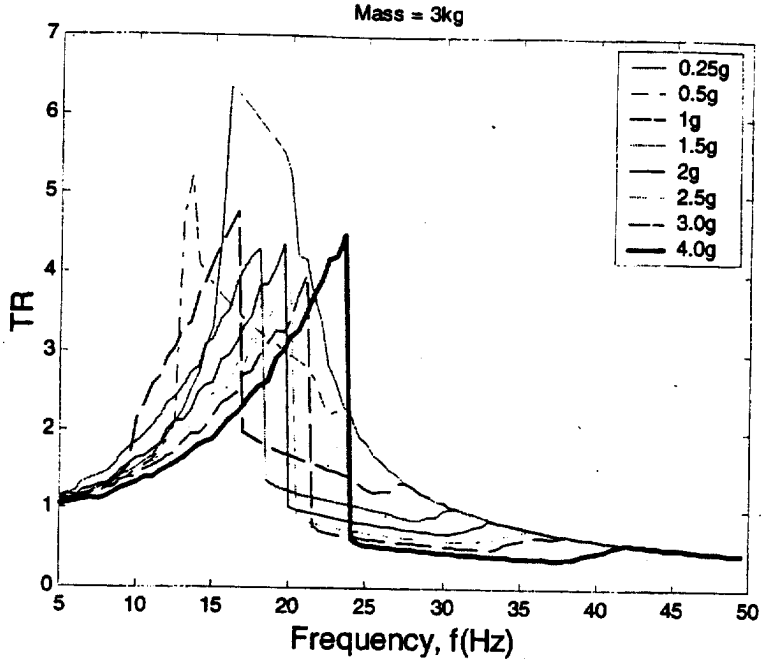


***Figure 23.*** *Effects of varying excitation on transmissibility for 3 kg mass.*

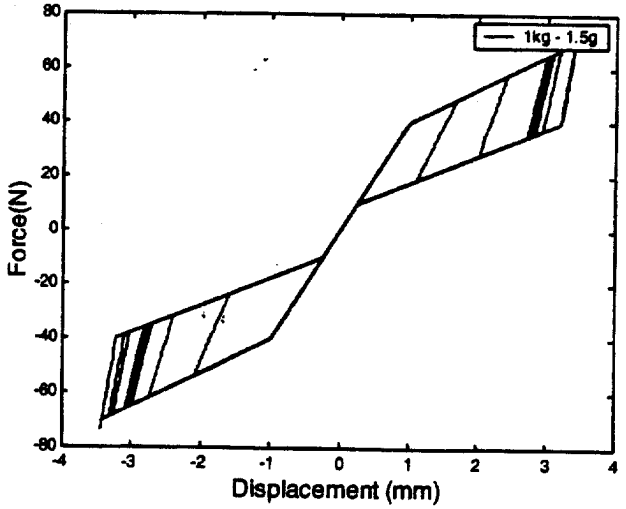


***Figure 24.*** *Force–displacement response for 1 kg mass with 1.5 g excitation.*

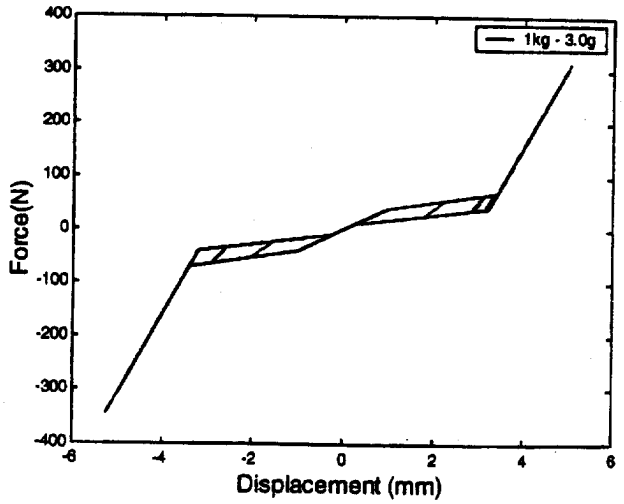


***Figure 25.*** *Force–displacement response for 1 kg mass with 3.0 g excitation.*

jump phenomenon is observed while undergoing a change in stiffness from $K_A$ to $K_{A\to M}$ or $K_F$, $K_M$ to $K_{M\to A}$ or $K_R$, $K_{M\to A}$ to $K_A$, $K_{A\to M}$ to $K_M$, $K_F$ to $K_M$ and $K_R$ to $K_A$.

Force–displacement response of the SMA spring for a 1 kg mass is shown in Figures 24 and 25 at resonance under different excitation levels to further validate the arguments given earlier on the effects of excitation on transmissibility. Figure 26 shows the variation of natural frequency with respect to excitation for different masses. Figure 27 shows the variation of natural frequency with respect to mass for different excitation levels. Higher natural frequencies meaning a stiffer response is observed at higher excitation due to complete phase transformation. A softer response is observed for partial phase transformations, whereas very low phase transformations due to low excitations give a response similar to linear spring having a stiffness close to the initial stiffness at small displacements.

## Multiple Pseudoelastic SMA Spring-mass System Based on the Prototype Device using Physically Based Simplified SMA Model

Based on the schematic of the actual prototype device shown in Figure 14, Figure 28 shows the effect of

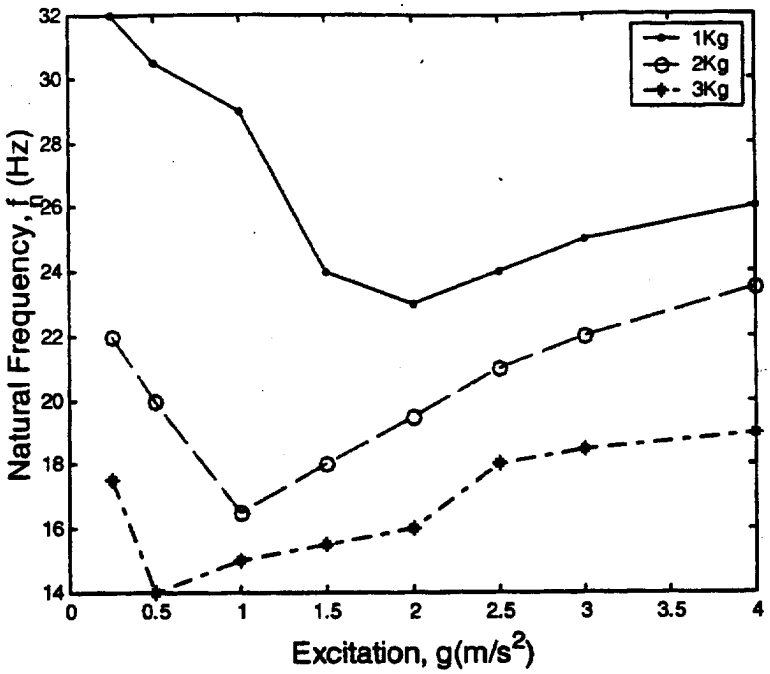


*Figure 26. Effects of varying excitation on natural frequency for different masses.*

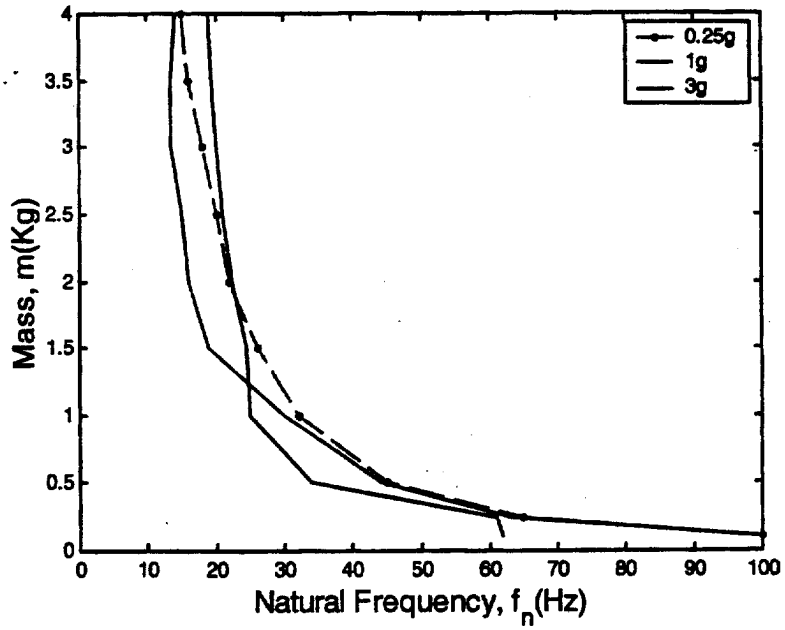


*Figure 27. Effects of varying mass on natural frequency for different excitation levels.*

varying the amplitude of base excitation on transmissibility of the SMA spring-mass system. These results are shown for a mass of 1 kg, a SMA spring configuration of two upper SMA springs and two lower SMA springs, and a precompression of 1 mm for all the springs. At lower amplitude of base excitation, the SMA spring-mass system exhibits resonance at a frequency of approximately 66 Hz, similar to the transmissibility of a linear system which is shown in Figure 28 by the line labeled "analytical". This can be explained by looking at the force–displacement diagram for one of the SMA springs, as shown in Figure 29. For an excitation amplitude of 0.1 g, it is observed that after a few loading cycles, the SMA spring repeatedly loads and unloads along a path having a stiffness of approximately 43 kN/m, giving a combined total stiffness of approximately 172 kN/m. For a mass of 1 kg, this equates to a natural frequency of approximately 66 Hz. As the excitation amplitude increases, the decrease in stiffness and hysteresis of the SMA's pseudoelasticity begin

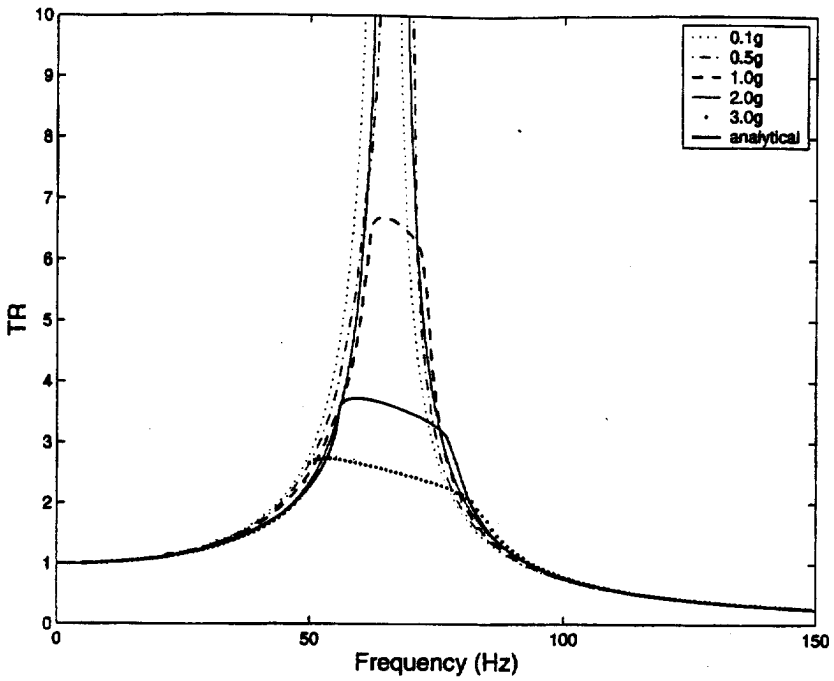


***Figure 28.*** *Transmissibility of SMA spring-mass system with different amplitude of base excitation for 1 kg mass.*

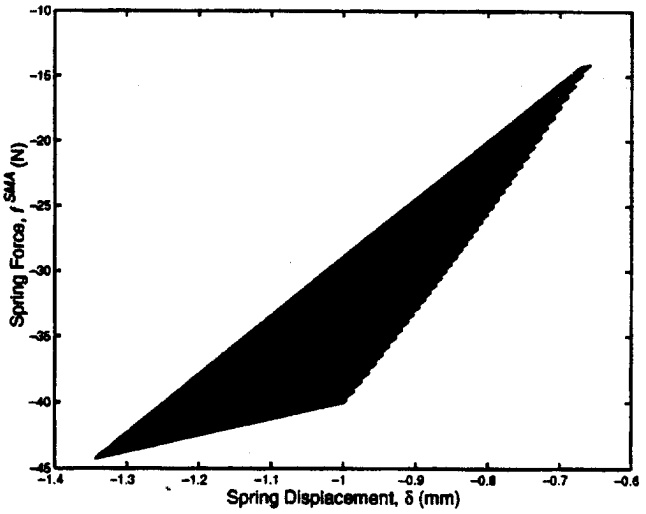


***Figure 29.*** *Force–displacement response for a SMA spring for the system with 1 kg mass and 0.1 g excitation amplitude.*

to contribute to a reduction in the resonant amplitude of the system. Figure 30 gives the force–displacement history for an excitation amplitude equal to 0.5 g at the natural frequency. A wider hysteresis loop is observed due to increased phase transformation, which is a result of higher excitation amplitude, and results in a lower transmissibility (see Figure 28). Figure 31, with a 2.0 g excitation amplitude, shows an even wider hysteresis which again results in a lower transmissibility.

Figure 32 shows the system response (displacement history) for 0.1 g excitation amplitude at resonance and is similar to the response of a linear spring due to the lack of phase transformation, which results in a linear force–displacement relationship. At frequencies greater than resonance frequencies, the system dynamics allow for significant reductions in transmissibility, as shown in Figure 33.

From these results, it can be surmised that the greatest benefit of SMA pseudoelasticity can be gained for this system under higher loading levels and near the resonant frequency of the system. It is also important to understand that in order to have vibration isolation with SMA springs, the SMA springs should undergo large amplitude displacement that will result in phase transformation. This will allow the system to operate

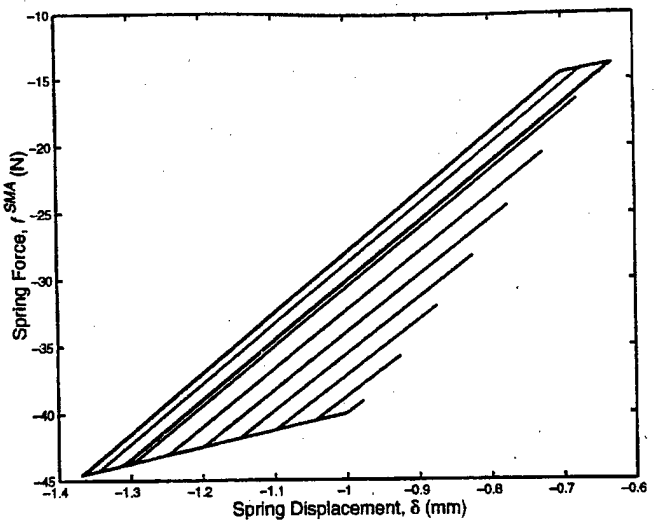


***Figure 30.*** *Force–displacement response for a SMA spring for the system with 1 kg mass and 0.5 g excitation amplitude.*

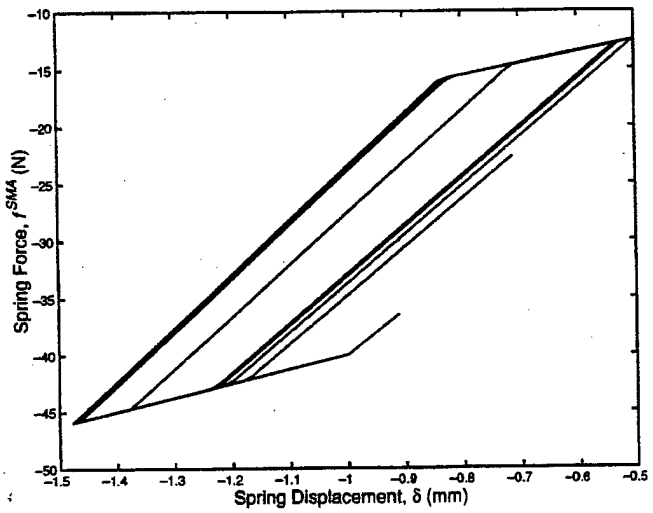


***Figure 31.*** *Force–displacement response for a SMA spring for the system with 1 kg mass and 2.0 g excitation amplitude.*

with a lowered effective spring stiffness, due to the pseudoelastic effect, and will allow the inherent hysteresis present in the SMAs to provide energy dissipation. In other words, SMA force–displacement response should be as close as possible to the major loop behavior discussed earlier in order to have the most effective vibration isolation. The following results will further explore the effect of excitation amplitude, system mass, and spring configuration on system response and transmissibility.

Figure 34 shows the effect of increasing mass on transmissibility. Increasing the mass reduces the resonant frequency of the system and it increases the amount of phase transformation as the SMA springs are subjected to higher loads for the same amount of relative displacement. This is demonstrated by the similarity between the force–displacement response for a SMA spring for a system with 3 kg mass and 0.5 g base excitation shown in Figure 35 and the force–displacement of the 1 kg mass system with 2.0 g excitation shown previously in Figure 31.

The effect of changes in the spring configuration is illustrated in Figure 36, resulting in a predictably lower resonance frequency for the system with fewer springs due to the lower overall stiffness. It should be noted that for all of these cases, only a relatively small amount of pseudoelasticity is observed, especially when compared to the complete major loop response. For comparison, the major loop force–displacement relationship and the force–displacement histories shown in Figures 29 and 31 are plotted together in Figure 37. It is evident that greater benefit could be gained from the pseudoelastic effect if larger portions of the force–displacement relationship could be exploited.

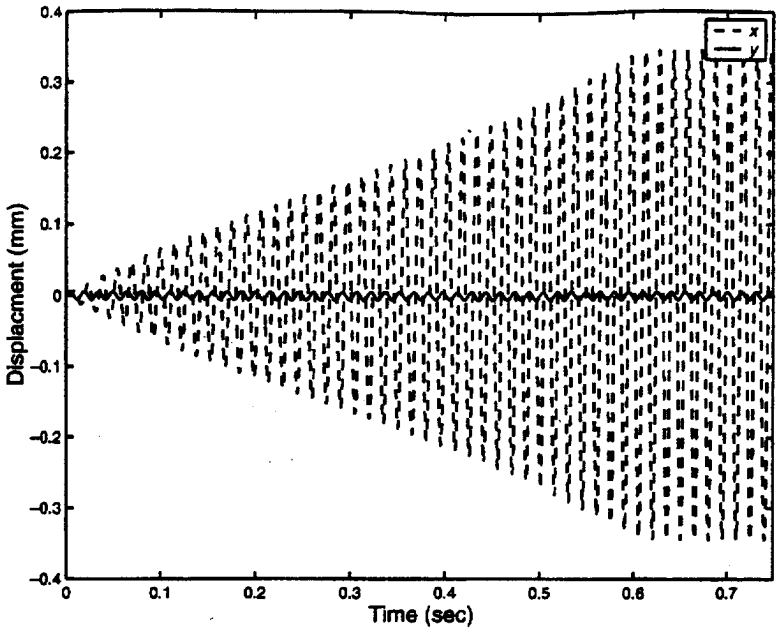


***Figure 32.*** *System response at resonance for 1 kg mass and 0.1 g excitation.*

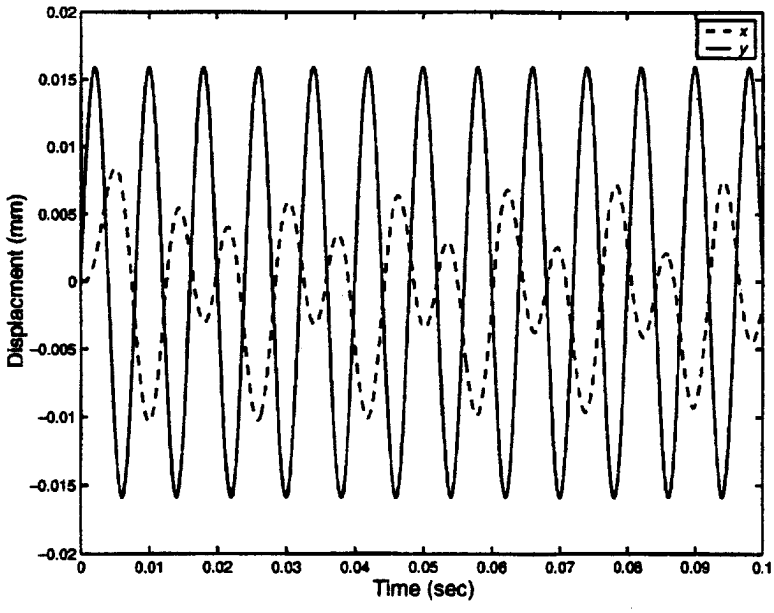


***Figure 33.*** *System response for 1 kg mass, 4 springs, 1.0 g excitation amplitude showing reduction in transmissibility utilizing SMAs (125 Hz).*

**Multiple Pseudoelastic SMA Spring-mass System Based on the Prototype Device using the Preisach model**

Figure 38 shows the effect of varying the amplitude of base excitation on transmissibility of the SMA spring-mass system using the Preisach model. These results are shown for the same mass, SMA spring configuration and precompression as discussed in the previous section and shown in Figure 14. At lower amplitude of base excitation, the SMA spring-mass system exhibits resonance at a frequency of approximately 48 Hz, similar to the transmissibility of a linear system which is shown in Figure 38 by the line labeled "analytical". This can be explained by looking at the force–displacement diagram for one of the SMA springs, as shown in Figure 39. For an excitation amplitude of 0.1 g, it is observed that after a few loading cycles the SMA spring repeatedly loads and unloads along a path having a stiffness of approximately 23 kN/m, giving a combined total stiffness of approximately 92 kN/m. For a mass of 1 kg, this equates to a natural frequency of approximately 48 Hz. As the excitation amplitude increases, the decrease in stiffness and hysteresis of the SMA's pseudoelasticity begin to contribute to a reduction in

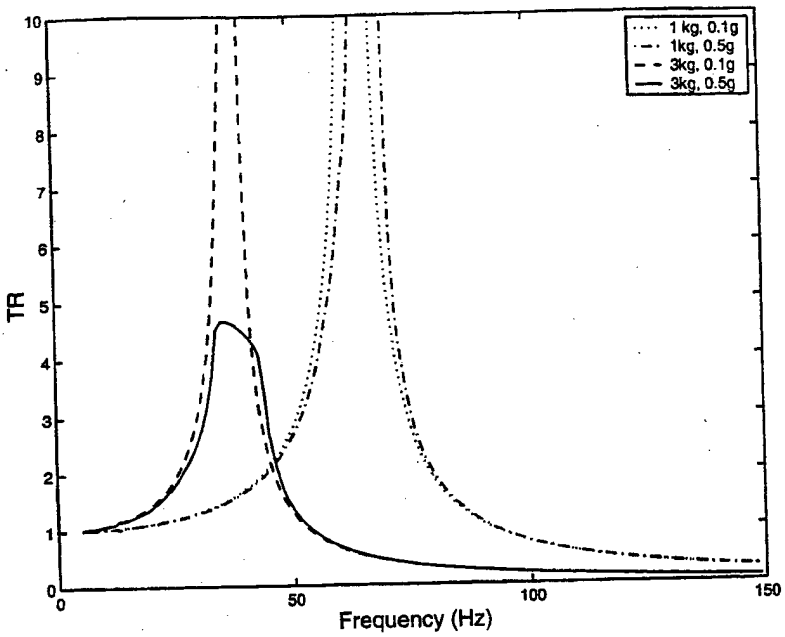


**Figure 34.** *Comparison of transmissibility of SMA spring-mass system for systems with 1kg and 3kg mass and 0.1g and 0.5g excitation amplitudes.*

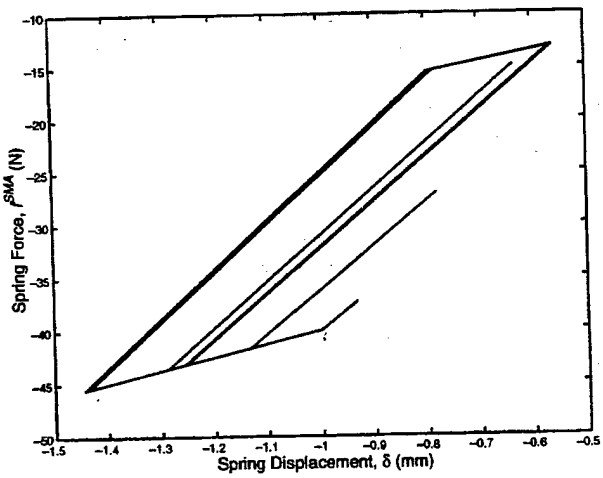


**Figure 35.** *Force-displacement response for a SMA spring for the system with 3 kg mass and 0.5 g excitation amplitude.*

the resonant amplitude of the system. The difference in the natural frequency for the given system solved by using the simplified model and the Preisach model is due to the differences in predicting the SMA tube response by both the models. These differences have been addressed in the next section.

Figure 40 gives the force–displacement history for an excitation amplitude equal to 0.5 g at the natural frequency. A wider hysteresis loop is observed due to increased phase transformation, which is a result of higher excitation amplitude, and results in a lower transmissibility (see Figure 38).

Figure 41 shows the system response (displacement history) for 0.1 g excitation amplitude at resonance and is similar to the response of a linear spring due to the lack of phase transformation, which results in a linear force–displacement relationship. At frequencies greater than resonance frequencies, the system dynamics allow for significant reductions in transmissibility, as shown in Figure 42. From these results and the results presented in the previous section, it can be seen that the greatest benefit of SMA pseudoelasticity can be gained for this system under higher loading levels and near the resonant frequency of the system. It is also important to understand that in order to have vibration isolation with SMA springs, the SMA springs should undergo large amplitude displacement that will result in phase transformation. This will allow the system to operate with a lowered effective spring stiffness, due to the pseudoelastic effect, and will allow the inherent hysteresis present in the SMAs to provide energy dissipation. The SMA force–displacement response should be as close as possible to the major loop behavior as discussed earlier in order to have the most effective vibration isolation.

Effect of increasing mass on transmissibility using the Preisach model are the same as in the case of the simplified model. Increasing the mass reduces the resonant frequency of the system and it increases the amount of phase transformation as the SMA springs are subjected to higher loads for the same amount of relative displacement. The effect of changes in the spring configuration results in a predictably lower resonance frequency for the system with fewer springs due to the lower overall stiffness. Illustrations on effects of changing mass and spring configurations on system transmissibility, using the Preisach model show the same trend as shown in the case of using the simplified model

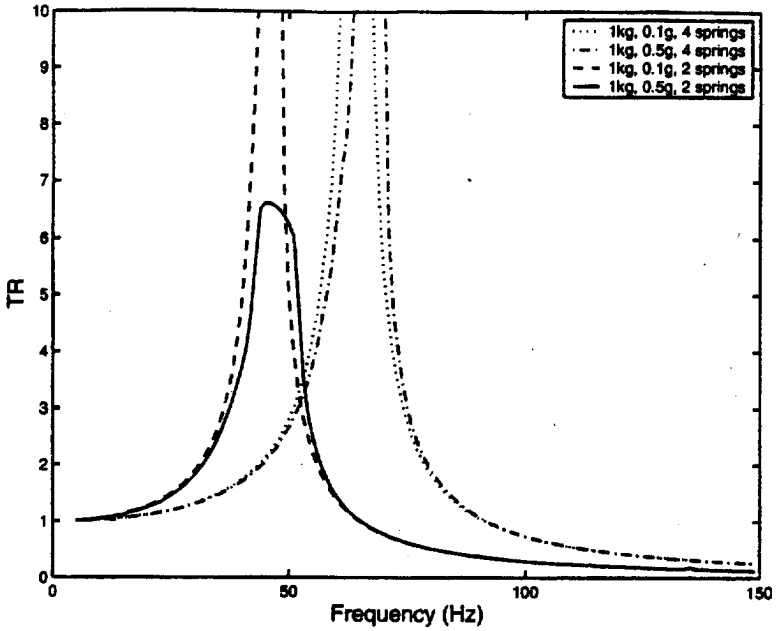


***Figure 36.*** *Comparison of transmissibility of SMA spring-mass system for system with 1kg, 0.1g excitation amplitude, and 0.5g excitation amplitudes and 2 or 4 springs.*

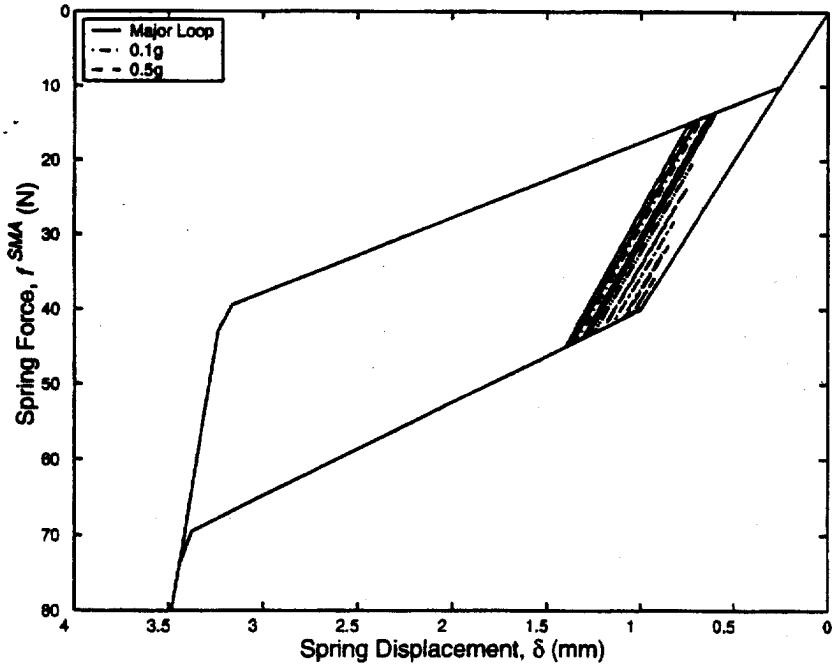


***Figure 37.*** *Comparison of major loop hysteresis to minor loop hysteresis induced by system motion for several cases.*

and have been omitted to avoid repetition. It should be noted that, as in the case of simplified model, for all of these cases using the Preisach model, only a relatively small amount of pseudoelasticity is observed, especially when compared to the complete major loop response. For comparison, the major loop force–displacement relationship and the force–displacement histories shown in Figures 39 and 40 are plotted together in Figure 43. It is evident that greater benefit could be gained from the pseudoelastic effect if larger portions of the force–displacement relationship could be exploited.

### Multiple Pseudoelastic SMA Spring-mass System Based on Prototype Device using the Preisach Model Identified from Simplified Model

The difference in the natural frequency for the given system solved by using the simplified model and the Preisach model is due to the differences in predicting

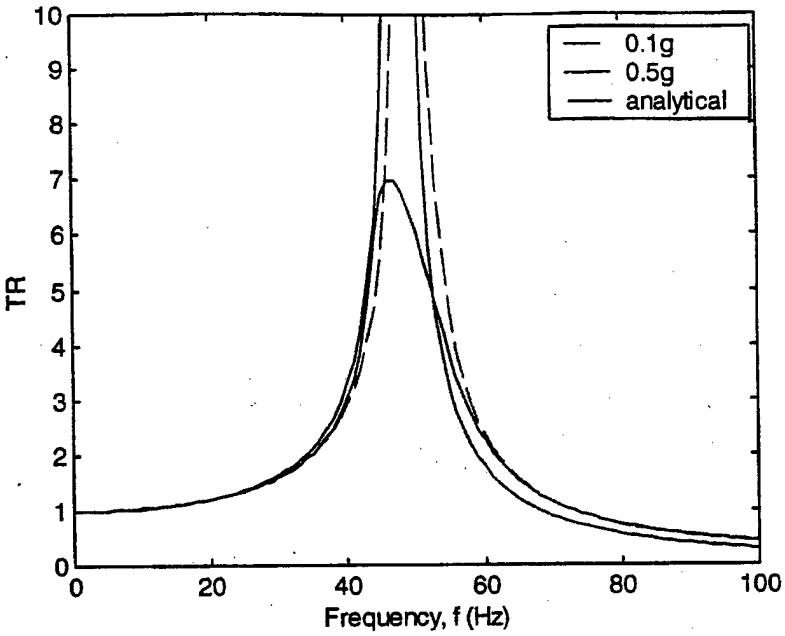


**Figure 38.** *Transmissibility of SMA spring-mass system with different amplitude of base excitation for 1 kg mass.*

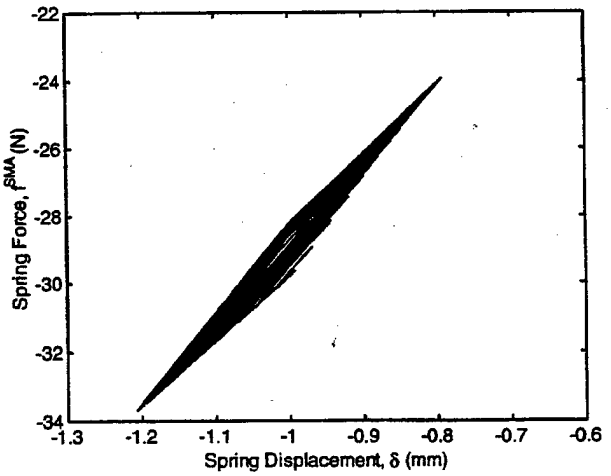


**Figure 39.** *Force–displacement response for a SMA spring for the system with 1 kg mass and 0.1 g excitation amplitude.*

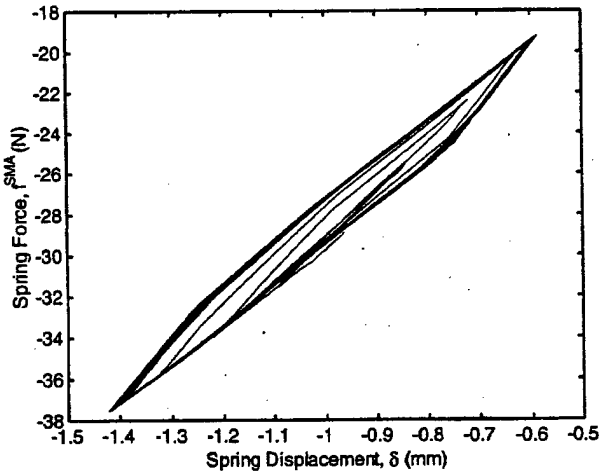


**Figure 40.** *Force–displacement response for a SMA spring for the system with 1 kg mass and 0.5 g excitation amplitude.*

the SMA tube response by both the models. These differences are apparent while predicting the major loop and especially in the minor loop response of the SMA tubes. Figures 26 (Part I), 3 and Figures 16 (Part I) show the calibrated simplified model and the Preisach model along with the minor loop behavior. It is important to note that for partial phase transformations modeled using the simplified model, the SMA spring elements load and unload along a stiffness which is calculated using a rule of mixtures on the compliance (see Part I), hence the minor loop stiffness varies linearly between the stiffness of austenite and martensite phases. Where as, in the case of the Preisach model, the spring elements load and unload along a stiffness given by the actual experimental response of the tubes (see Part I) which is closer to the major loop stiffness during transformation and less stiffer than the minor loop stiffness given by the simplified model. The softer response given by the Preisach model results in having a lower natural frequency for the system solved in the previous two sections.

To validate the above observation, the Preisach model identified from the simplified model and discussed in Part I has been used to solve the same system as discussed in the previous two subsections. Figure 44 shows the effect of varying the amplitude of base excitation on transmissibility of the SMA spring-mass system. At lower amplitude of base excitation, the SMA

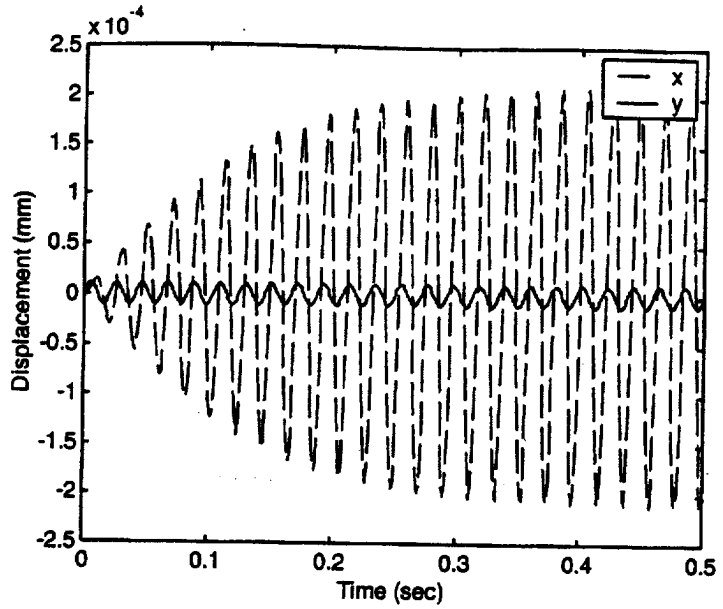


**Figure 41.** *System response at resonance for 1 kg mass and 0.1 g excitation.*

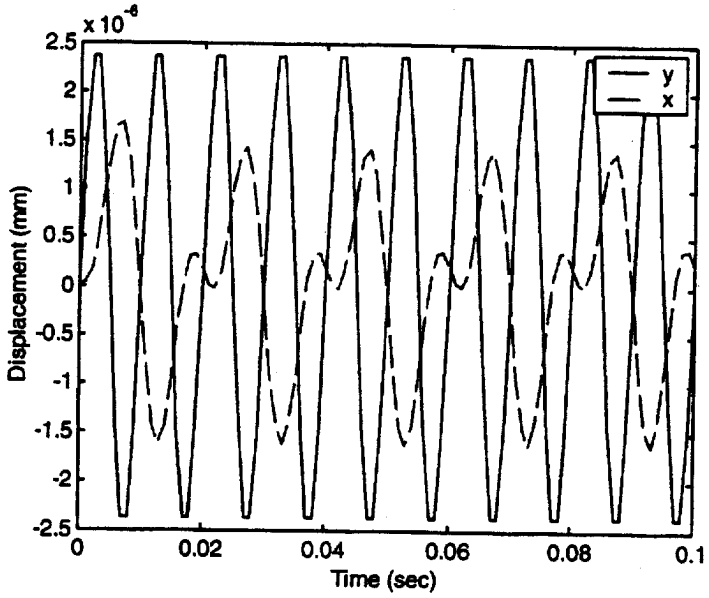


**Figure 42.** *System response for 1 kg mass, 4 springs, 1.0 g excitation amplitude showing reduction in transmissibility utilizing SMAs (100 Hz).*

spring-mass system exhibits resonance at a frequency of approximately 64 Hz, which is almost identical to the resonance frequency given by using the simplified model. Similar behavior is seen while observing the force–displacement diagrams for one of the SMA spring elements. For an excitation amplitude of 0.1 g (Figure 45), it is observed that after a few loading cycles the SMA spring repeatedly loads and unloads along a path having a stiffness of approximately 42 kN/m, giving a combined total stiffness of approximately 168 kN/m. For a mass of 1 kg, this equates to a natural frequency of approximately 64 Hz which is very close to the natural frequency given by the simplified model.

As the excitation amplitude increases, the decrease in stiffness and hysteresis of the SMA's pseudoelasticity begin to contribute to a reduction in the resonant amplitude of the system. Figure 46 gives the force–displacement history for an excitation amplitude equal to 0.5 g at the natural frequency. A wider hysteresis loop is observed due to increased phase transformation, which is a result of higher excitation amplitude, and results in a lower transmissibility (see Figure 44). Figure 47, with a 2.0 g excitation amplitude, shows an even wider hysteresis which again results in a lower transmissibility.

The results obtained using the Preisach model identified from the simplified model validates the above observations regarding the differences in predicting

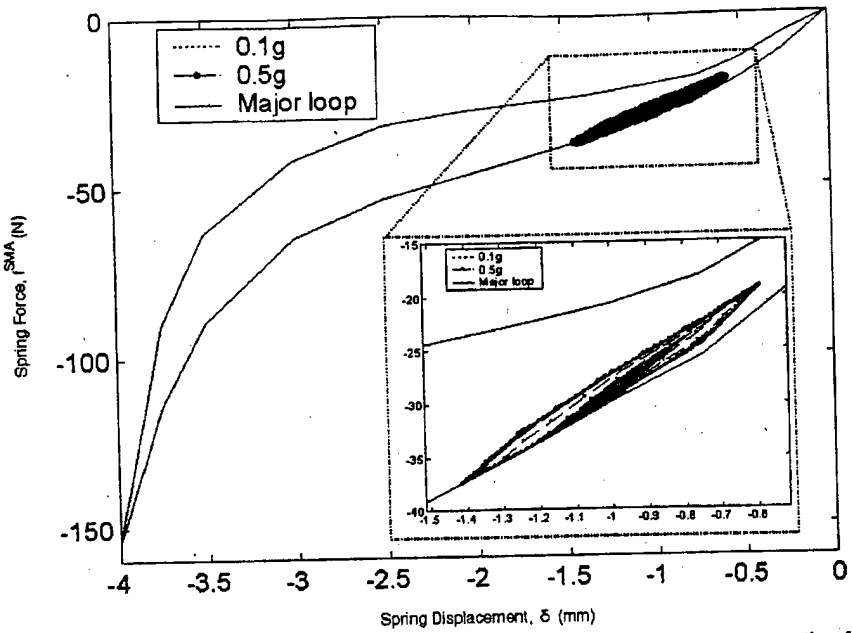


**Figure 43.** *Comparison of major loop hysteresis to minor loop hysteresis induced by system motion for several cases.*

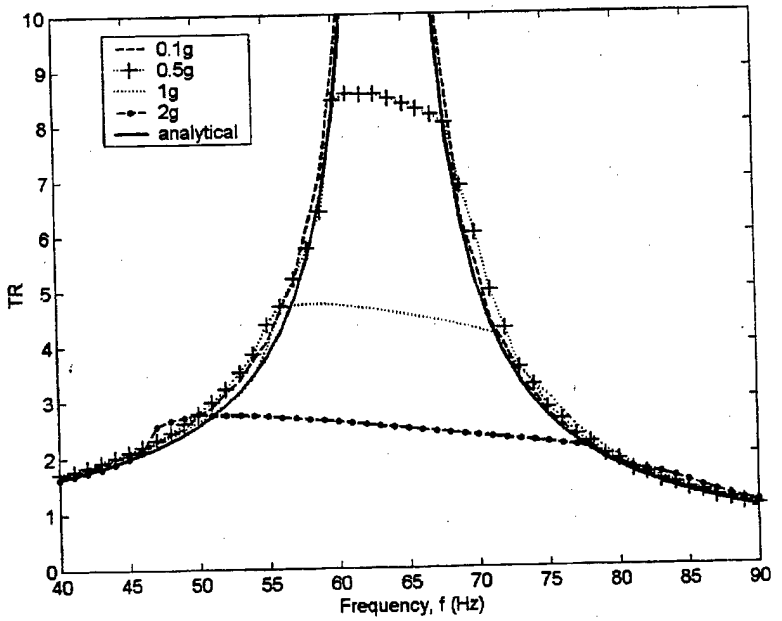


**Figure 44.** *Transmissibility of SMA spring-mass system with different amplitude of base excitation for 1 kg mass.*

SMA spring element response using the simplified and the Preisach model identified from actual experimental data.

The following section compares the actual experimental results for the SMA-based passive vibration isolation device along with its numerical simulations using the simplified and the Preisach model and discusses the possible sources of errors and discrepancies.

## COMPARISON OF SIMPLIFIED MODEL AND PREISACH MODEL PREDICTIONS WITH ACTUAL EXPERIMENTAL RESULTS

In order to perform correlations between the experimental results and their numerical simulations using the two models, a representative number of cases were simulated and compared (Lagoudas et al., 2002). Table 1 shows a tabulation of different experimental cases along

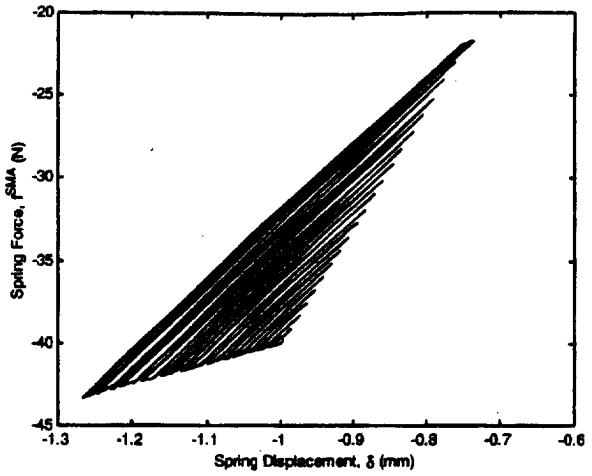


***Figure 45.*** *Force–displacement response for a SMA spring for the system with 1 kg mass and 0.1 g excitation amplitude.*

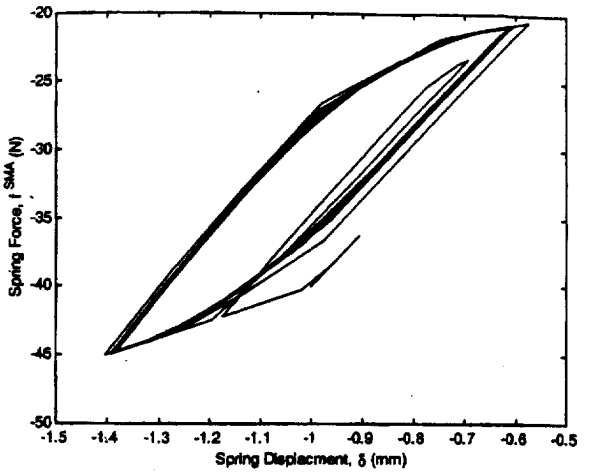


***Figure 47.*** *Force–displacement response for a SMA spring for the system with 1 kg mass and 2.0 g excitation amplitude.*

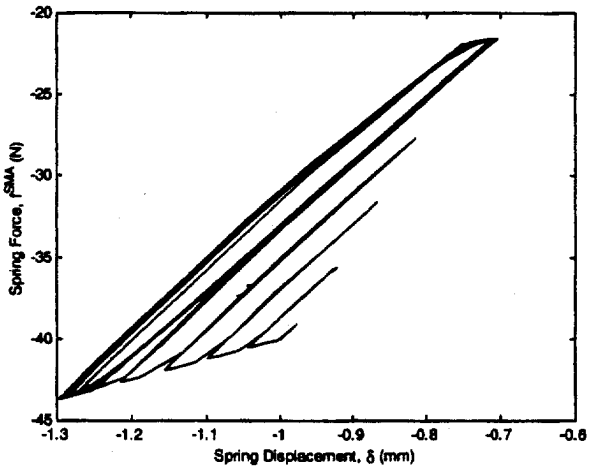


***Figure 46.*** *Force–displacement response for a SMA spring for the system with 1 kg mass and 0.5 g excitation amplitude.*

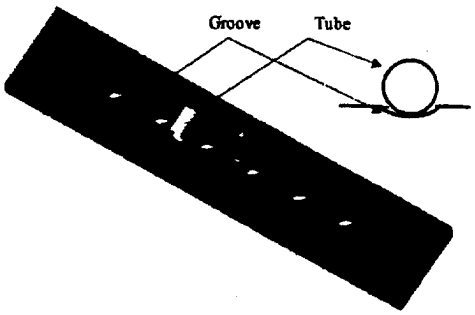


***Figure 48.*** *Magnification of base plate groove along with a tube.*

with variation of parameters effecting the system behavior. Number of compression springs (tubes), amount of precompression as percentage of tube diameter (as the tubes were loaded in a transverse direction), isolation mass, and amplitude of base excitation were the considered parameters during the dynamical testing of the vibration isolation device (Mayes, 2001; Mayes and Lagoudas, 2001).

Cases 2, 7–10 were considered for correlation of experimental results with the simplified and Preisach models based numerical simulations of the system. These cases were chosen as they represented the spectrum of experiments that were conducted and correlations obtained from these cases can be used to generalize important results for future work involving SMA-based passive isolation devices.

The results presented below show that there is significant agreement between the experimental cases and the numerical simulations and the effect of the precompression is shown to drastically affect the response of the system. The experimental results presented in Mayes and Lagoudas (2001) and Mayes (2001) have also shown that the precompression can greatly shift the resonant frequency of the system. Experimental results of Cases 1 and 9 and Cases 6 and 10 show the effect of varying precompression on the system behavior. Inadequacies in the experimental design prevented absolute certainty as to the amount of precompression and although every effort was made to ensure the correct amount of precompression had been applied to the system, it is evident that even the slightest change in the precompression will alter the system response greatly. An important factor in these uncertainties was that the experiment was reassembled during various cases and as a result the same level of precompression was not achieved for all of the cases.

In comparing experimental and theoretical results it was found that a correlation could be made if the precompression value given to the numerical simulation using the simplified model was set equal to approximately 2.3 mm, or roughly 37.5% of the total transverse displacement of the tube diameter. However, in the case of the Preisach model, a better correlation could be made when the precompression was set equal to 2.5 mm for low precompression cases and about 3.0 mm for the

high precompression cases. These factors were found consistent over all the simulated cases for the respective models. For all the cases, the precompression had to be increased for both the models, leading to the understanding that the over all structural response of the experiment was much stiffer than expected. The amount of precompression increased using the Preisach model was even more compared to the simplified model due to the difference in predicting minor loop behavior by both of these models which has been discussed in detail in Khan (2002).

Possible explanation for having a consistent factor for the precompression can be attributed to the groove dimensions in the experimental setup shown in Figure 1. A magnification of the grooves cut into the base plate along with a tube is shown in Figure 48. The width of these grooves were less than half the circumference of the tubes, which caused local stiffening of tubes while undergoing deformations during loading/unloading and hence increased the overall stiffness of the structure. This local stiffening was consistently observed during the experiment but is not accounted for in the modeling

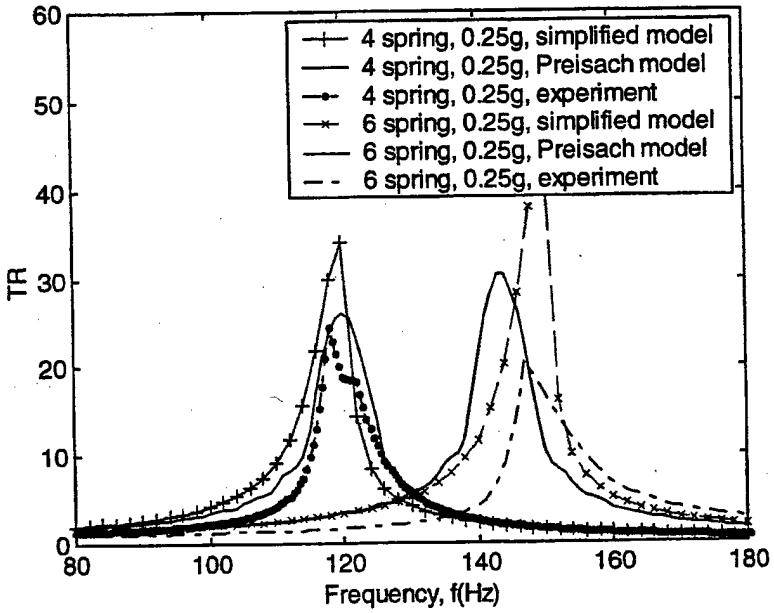


**Figure 49.** *Comparison of numerical simulation with experimental results for cases 9 and 10.*

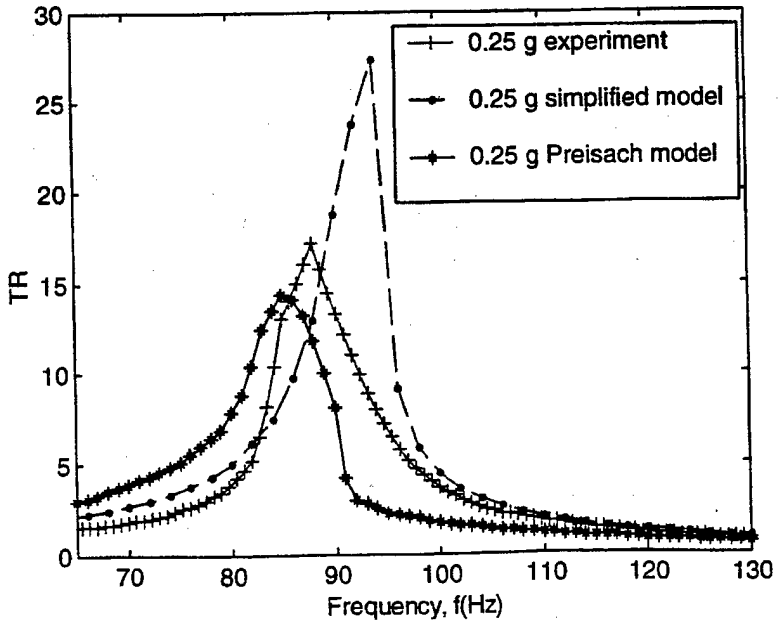


**Figure 50.** *Comparison of numerical simulation with experimental results for case 2 with 0.25 g excitation amplitude.*

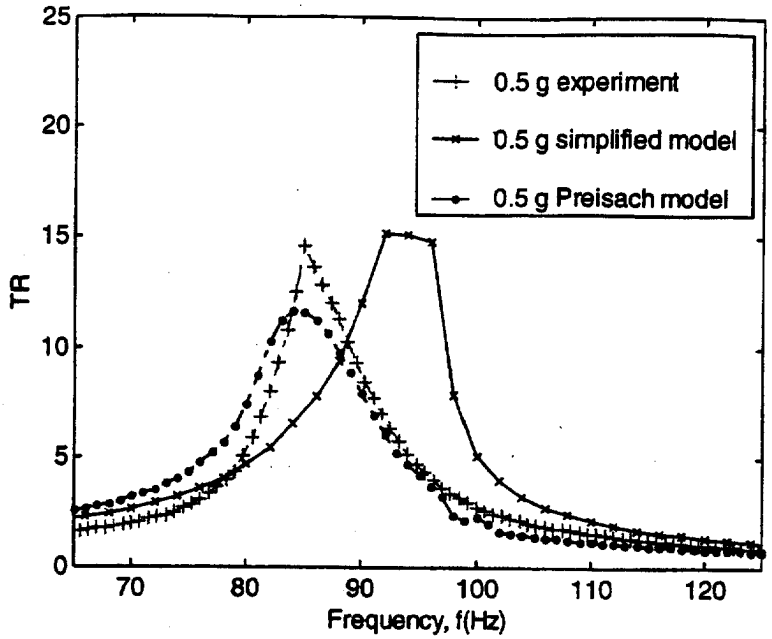


***Figure 51.*** *Comparison of numerical simulation with experimental results for case 2 with 0.5 g excitation amplitude.*

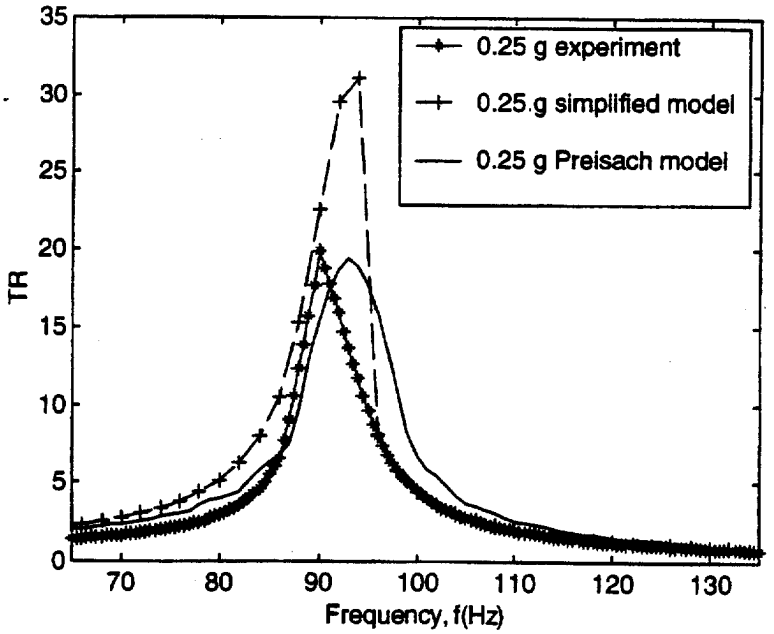


***Figure 52.*** *Comparison of numerical simulation with experimental results for case 7 with 0.25 g excitation amplitude.*

of the experiment. Response of other components like mounts and bolts used for the experimental setup having relatively higher stiffness' were also not modeled.

Presented in Figures 49–55 are the results of the numerical simulation for Cases 9 and 10 and Cases 2, 7, and 8, along with the experimental results for the respective case. For all cases, the resonant amplitude of the experimental data is less than that for the numerical simulation using the simplified model. However, this is not true in the case of the Preisach model simulations. Additionally, for every case there is a good correlation between the resonant frequency predicted by the simulation and the resonant frequency measured during the experiment. For Figure 49, the effect of changes in precompression are seen to have dramatic effect in both the experiment and the numerical simulation. For both the experimental data and the simulation results, relatively small increases in the precompression are shown to increase the resonant frequency greatly. This is an important result as it shows that SMA-based

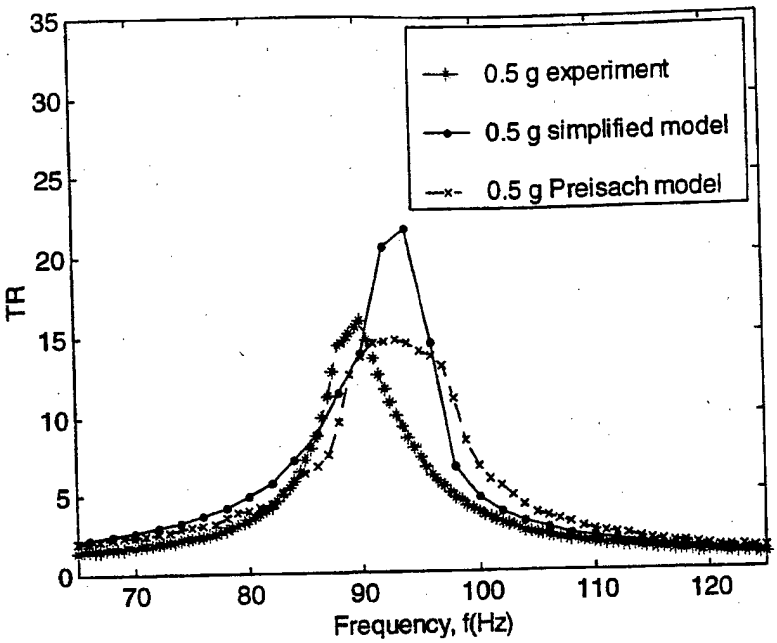


*Figure 53. Comparison of numerical simulation with experimental results for case 7 with 0.5 g excitation amplitude.*

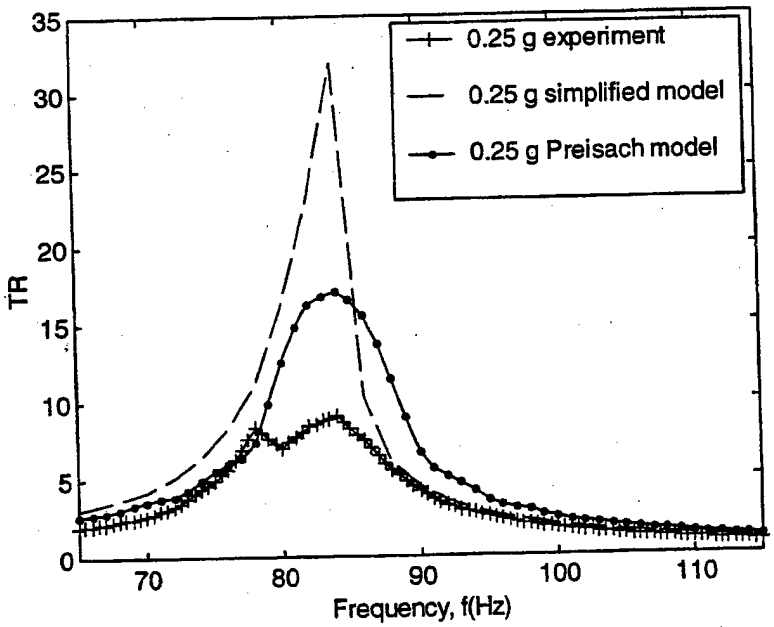


*Figure 54. Comparison of numerical simulation with experimental results for case 8 with 0.25 g excitation amplitude.*

isolation devices lend themselves well to being developed as tuneable isolation devices capable of providing isolation for various conditions and loads.

At frequencies much greater than the resonant frequency, the modeled and experimentally obtained values for transmissibility agree very well. From simulation in this region, it seems that the SMA tubes are functioning as linear springs, that is without transformation. This should prove beneficial as it would prevent the inherent damping present during transformation from degrading the performance of the isolator. Finally, the same trends of decreasing resonant amplitude for increasing loading are seen in both the simulation data and the experimental data. This is promising even though the magnitudes of the reductions are not in agreement since simulation of this region indicates that the reduction in amplitude is due to larger deformations of the SMA tubes, meaning increase in hysteresis, which results in more energy being absorbed by the isolation device. Combined with the observations

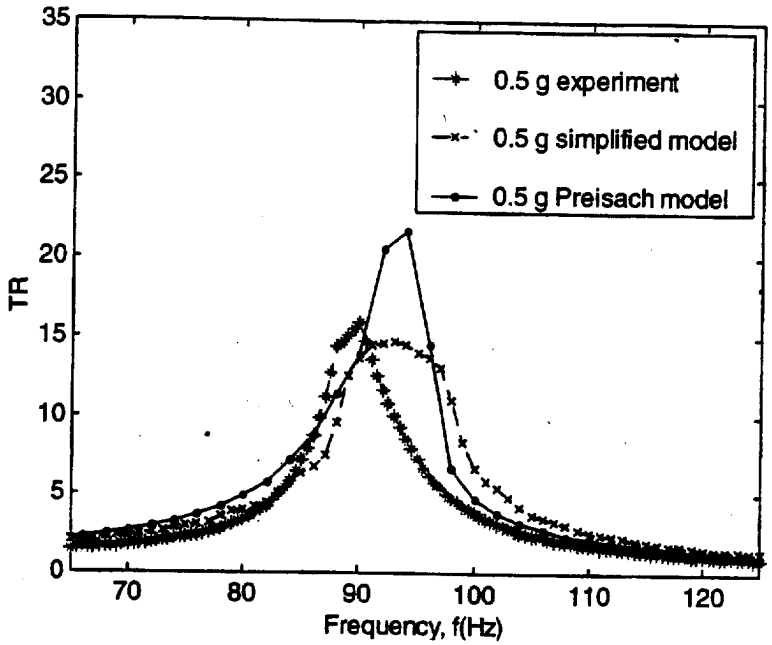


**Figure 55.** *Comparison of numerical simulation with experimental results for case 8 with 0.5 g excitation amplitude.*

of nearly linear behavior at frequencies much greater than the resonant frequency, this observation is very important because it indicates that the SMA isolation device will be capable of providing sufficient damping at resonance where high damping is beneficial and minimal damping at higher frequencies where damping degrades isolation performance.

## CONCLUSIONS

In this two-part paper series, a computationally efficient simplified SMA model and an equally efficient Preisach model for force–displacement response of pseudoelastic SMA tubes (modeled as nonlinear hysteretic spring elements) have been developed (Part I). These models have been utilized in Part II of this work to numerically simulate the response of a SDOF dynamic system having pseudoelastic SMA spring elements for damping and vibration isolation. A computationally efficient numerical simulation tool has been developed for the purpose of performing extensive parametric studies for design of a SDOF SMA-based vibration isolation system. Simulation results have shown that damping and vibration isolation was greatly dependent on the relative displacement of SMA spring elements, as the relative displacement directly affected the extent of phase transformation of the pseudoelastic SMA springs. Variable damping and tunable isolation response have been shown as major benefits of SMA pseudoelasticity and it has been shown that variable damping and tunable vibration isolation response can be achieved based on a combination of different system parameters like excitation level, mass and precompression of pseudoelastic SMA spring elements. A significant conclusion of this study has been that SMA-based damping and vibration isolation devices have the potential to overcome performance trade-offs inherent in typical softening spring-damper vibration isolation systems.

In addition to the theoretical work presented here, a significant experimental effort has also been performed to expand the understanding and knowledge of dynamical systems based on SMAs. This effort included the design and testing of a novel prototype SMA-based isolation device using SMA pseudoelastic tubes as isolators. Numerous tests were conducted to explore the response of the vibration isolation device. The developed models have also been used to simulate the response of the prototype device. Both models have shown good compatibility with the experimental results. The Preisach model gave relatively accurate results due to close proximity in modeling actual SMA tube behavior. However, for a qualitative parametric study, the simplified model was found to be more useful as it was motivated from the constitutive response of SMAs and hence, could easily incorporate different changes in the nonlinear hysteretic structural response of SMAs. Based on the work presented here, especially on the outcome of the numerical studies and the experimental correlations, it appears that SMAs could be used successfully in damping and passive vibration isolation devices.

## ACKNOWLEDGMENT

The authors would like to acknowledge the financial support from the Air Force Office of Scientific Research, Grant No. F49620-01-1-0196 and the U.S. Air Force – Kirtland AFB, PO No. 00-04-6837 under the administration of Syndetix, Inc. The authors would also like to thank Peter Popov for facilitating implementation of the Newmark integration scheme.

## NOMENCLATURE

$\alpha$ = integration weighting factor
$\ddot{x}$ = acceleration of mass
$\ddot{x}_n$ = acceleration at timestep $n$
$\ddot{x}_{n+1}$ = acceleration at timestep $n+1$
$\Delta t$ = time increment
$\delta$ = spring displacement
$\delta_l$ = displacement of springs below the mass
$\delta_u$ = displacement of springs above the mass
$\dot{x}_n$ = velocity at timestep $n$
$\dot{x}_{n+1}$ = velocity at timestep $n+1$
$\gamma$ = integration weighting factor
$A$ = austenite phase
$a$ = input loading level
$f$ = excitation frequency
$f^{SMA}$ = force exerted by SMA spring
$f_l^{SMA}$ = force exerted by springs below the mass
$f_u^{SMA}$ = force exerted by springs above the mass
$f_n$ = natural frequency of the system
$g$ = acceleration due to gravity
$K_A$ = stiffness of austenite phase
$K_M$ = stiffness of martensite phase
$M$ = martensite phase
$m$ = mass to be isolated
$N_l$ = number of springs below mass
$N_u$ = Number of springs above mass
$t$ = time
$TR$ = transmissibility
$t_n$ = timestep $n$
$x$ = displacement of mass
$x_n$ = position at timestep $n$
$x_{n+1}$ = position at timestep $n+1$
$Y$ = magnitude of displacement
$y$ = base displacement

## REFERENCES

Bernardini, D. and Vestroni, F. 2002. "Non-isothermal Oscillations of Pseudoelastic Devices", *International Journal of Non-Linear Mechanics*, Submitted for publication.

Collet, M., Foltete, E. and Lexcellent, C. 2001. "Analysis of the Behavior of a Shape Memory Alloy Beam under Dynamic Loading", *European Journal of Mechanics and Solids*, 20:615–630.

Feng, Z.C. and Li, D.Z. July 1996. "Dynamics of a Mechanical System with a Shape Memory Alloy Bar", *Journal of Intelligent Material Systems and Structures*, 7:399–410.

Hughes, T.J. 1987. *The Finite Element Method*, Prentice-Hall, Inc., Englewood Cliffs, NJ.

Khan, M.M. January 2002. "Modeling of Shape Memory Alloy (SMA) Spring Elements for Passive Vibration Isolation using Simplified SMA Model and Preisach Model". Master's Thesis, Texas A&M University, College Station,TX.

Lacarbonara, W., Bernardini, D. and Vestroni, F. September 2001. "Periodic and Nonperiodic Thermomechanical Reponses of Shape-memory Oscillators", In: *Proc. Conf. ASME Design Engineering Technical Conference*, Pittsburgh, PA.

Lagoudas, D.C., Khan, M.M. and Mayes, J.J. November 2001. "Modelling of Shape Memory Alloy Springs for Passive Vibration-isolation", In: *Proc. Conf. ASME International Mechanical Engineering Congress and Exposition*, New York, NY.

Lagoudas, D.C., Khan, M.M., Mayes, J.J. and Henderson, B.K. November 2002. "Parametric Study and Experimental Correlation of an SMA Based Damping and Passive Vibration Isolation Device", In: *Proc. Conf. ASME International Mechanical Engineering Congress and Exposition*, New Orleans, LA.

Mayes, J.J. December 2001. "Suitability of Shape Memory Alloys for Vibration Isolation with Application to Launch Vehicle Payloads", Master's Thesis, Texas A&M University, College Station, TX.

Mayes, J.J. and Lagoudas, D.C. August 2001. "An Experimental Investigation of Shape Memory Alloy Springs for Passive Vibration Isolation", In: *Proc. Conf. AIAA Space 2001 Conference and Exposition*, Albuquerque, NM, Submitted.

Meriovitch, L. 1975. *Elements of Vibation Analysis*, McGraw Hill Kogakusha, Ltd., Tokyo.

Nayfeh, A. H. and Mook, D. T. 1979. *Nonlinear Oscillations*, John Wiley & Sons, Inc., New York.

Newmark, N.M. 1959. "A Method of Computation for Structural Dynamics", *Journal of Engineering Mechanics Division*, ASCE 85, 67–94.

Otsuka, K. and Shimizu, K. 1986. "Pseudoelasticity and Shape Memory Effects in Alloys", *International Metals Review*, 31(3):93–114.

Wayman, C.M. 1983. "Phase Transformations, Nondiffusive", In: Cahn, R.W. and Haasen, P. (eds), *Physical Metallurgy*, pp. 1031–1075, North-Holland Physics Publishing, New York.

Yiu, Y.C. and Regelbrugge, M.E. April 1995. "Shape-memory Alloy Isolators for Vibration Suppression in Space Applications", In: *Proc. 36th AIAA/ASME/ASCE/AHS/ASC Conf. Structures, Structural Dynamics, and Materials*, AIAA-95-1120-CP.